DEVELOPMENT OF A DISSOLVED OXYGEN SENSOR FOR MARINE APPLICATIONS

by

Herveline GLEVER

Submitted for the Degree of

MASTER OF SCIENCE

Presented to

DUBLIN CITY UNIVERSITY

Research Supervisor

Dr. Colette McDonagh
School of Physical Sciences,
Dublin City University.

January 2000

Declaration

I hereby certify that this material, which I now submit for the assessment on the programme of study leading to award of M.Sc. in Applied Physics, is entirely my own work and has not been taken from the work of others save and to the extent that such work has been cited and acknowledged within the text of my work.

Signed:  date: 02/06/00

Acknowledgements

To Colette and Brian for giving me the opportunity to do this research.

To Jeff, Chris and Kevin for all the help and advice throughout this project.

To Eoin and Xavier my "super-cool" lab/officemates.

To all the past and present members of the Optical Sensors Group, and especially Optronics Ireland members for providing an enjoyable two years at DCU.

To all my friends, from Ireland and all over the world for making my life here so great.

A special thank to Roisin for all the support and unforgettable time we had together.

And finally to my parents and brothers for all their love.

Abstract

A dissolved oxygen sensor based on the fluorescence intensity quenching of a ruthenium dye complex, [Ru(II)-tris(4,7-diphenyl-1,10-phenanthroline)]$^{2+}$, which has been entrapped in a porous sol-gel film, is reported.

The aim of the project was to develop and test a portable instrument (prototype), based on a laboratory-developed sensor technique, for use in marine and inland seas. Issues for optimum sensor performance included stability and reproducibility of the prototype sensor measurements in deionised and marine water. Investigations to optimise the sensing films, such as leaching, thickness and coating of an additional optical barrier layer, are discussed. Measurements with the prototype and a laboratory test system are compared. Problems with temperature drift and slide insertion reproducibility were encountered. These effects were fully characterised and design improvements are suggested. Finally alternative approaches to intensity-based dissolved oxygen sensing are discussed.

Table of contents

Chapter 4: The sol-gel process and thin film fabrication

Chapter 5: Sensor characterisation instrumentation

Chapter 1: Oxygen in the environment

1.1 Introduction

The project is concerned with the design and testing of an optical dissolved oxygen sensor for use in lakes, rivers and the marine environment. This chapter highlights the importance of dissolved oxygen monitoring and water quality control.

1.2 Oxygen

Oxygen is essential for animal and plant life as the major requirement for respiration. Oxygen is 30 times less abundant in water (~ 10 mg/l) than in air, and can therefore become a limiting factor. Oxygen is soluble in water in direct proportion to the partial pressure in the gas phase and solubility decreases as temperature increases [1]. Oxygen enters the water by absorption directly from the atmosphere or by plant photosynthesis. It is removed by respiration of organisms and by organic decomposition. During respiration and decomposition, animals and plants consume dissolved oxygen and liberate carbon dioxide. Organic waste from municipal, agricultural and industrial sources may overload the natural system causing a serious depletion of the oxygen supply in the water. Waters rich in nutrients produce algae in quantity which upon decomposition deplete the oxygen supply. Fish kills are often associated with the process of eutrophication, which is an increase in the concentration of nutrients in the aquatic ecosystem. This can cause:

- an increased productivity of autotrophic green plants (which produce their own organic constituents from inorganic compounds utilising energy from sunlight or oxidation processes), leading to the blocking out of sunlight.
- elevated temperatures within the water body.
- depletion of the water's oxygen resources.
- increased algal growth.
- reduction in the level of and variety of fish and animal life.

Oxygen concentration increases as water temperature decreases and as turbulence and mixing in the water body increase. Thus a fast, shallow, turbulent stream has higher dissolved oxygen levels than a slow-moving, deep river. Many species have narrow tolerance ranges to oxygen and can only survive where levels are very high (>10 mg/l) [2], such as in cool, upland streams with a fairly fast current. The difference in tolerance to oxygen levels among invertebrate animals has been used in the development of biotic indices (the biotic components are the living components of an area), for identifying and monitoring organic water pollution and water quality.

Any kind of disturbance that reduces oxygen levels will have a dramatic effect on the functioning of freshwater communities and ecosystems.

1.3 Importance of dissolved oxygen

Pure water (H_2O) free from any substances dissolved in it, does not exist outside the laboratory, as natural water contains dissolved gases and salts. These substances are often the very factors which make the water suitable for particular beneficial uses. Water must have an adequate level of dissolved oxygen if fish are to thrive. The great majority of pollution instances on rivers are attributable to the depletion of the dissolved oxygen, leading to various highly undesirable effects. Again, drinking water without dissolved oxygen and with only a very low level of dissolved salts, is not very palatable: it is the level of salts in solution, as natural hardness, for example, which gives many waters their palatability.

1.4 Water quality

It is important in water management to know the concentration of the various constituents of water. Physicochemical assessment of water quality is usually based on five parameters: Biochemical Oxygen Demand (BOD), Ammonia, Nitrate, Phosphate, and Dissolved Oxygen (DO).

The biological oxygen demand (BOD) of a water sample based on the amount of dissolved oxygen in water is a good indication of water quality. A decrease in the amount of dissolved oxygen usually indicates the extent of pollution of the water

sample or the presence of organic waste. Fish, especially salmonid [game] fish, are very sensitive to water pollutants, and they will react increasingly unfavourably as the dissolved oxygen content of the water is lowered through pollution. However, the actual amount of dissolved oxygen present in even the cleanest water is extremely small. The solubility of oxygen in water at a temperature of 20 degrees Celsius is 9.2 milligrams oxygen per litre of water, i.e. little more than nine parts per million [ppm] at the level of water temperature one might find in a typical Irish summer. As there is an inverse temperature oxygen solubility relationship (Cf. Figure 1.1), the net amount of oxygen present in a river may be some 50 % greater in the winter than in the summer.

Around 9 ppm is, as stated, the maximum solubility of oxygen in water in summer. This level is more usually referred to as the 100 % saturation value at the actual temperature (which must be specified if saturation values are used). Saturation levels above 80 % are desirable if game fish are to thrive; for coarse fish the corresponding value is 55 % saturation (at summer temperature) [3]. Expressed in terms of concentrations (as ppm), the respective values are 7 ppm and 5 ppm. Thus quite small amounts of pollution will reduce the natural oxygen levels to the minimum desirable figures, and small increases in pollution will seriously disrupt fish life.

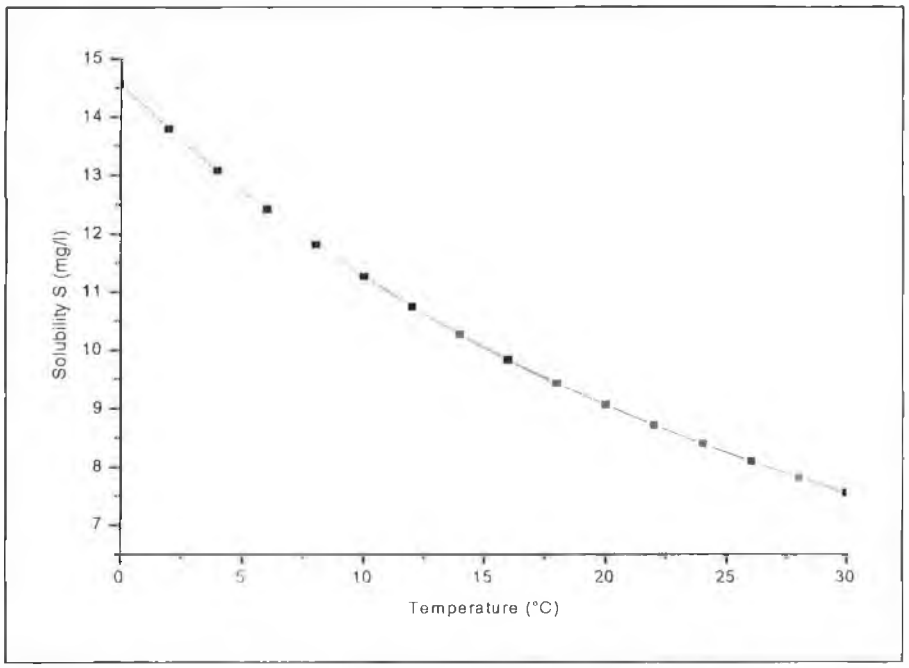

Figure 1.1: Dissolved oxygen solubility as a function of temperature [1]

1.5 How pollution takes effect

The majority of pollution instances in Ireland are caused by the sudden or continuing, accidental or deliberate, discharge of polluting materials which, on first consideration, might not seem harmful or offensive at all. Such pollution events are caused by the discharge of non toxic organic matter waste from creameries, sewage, slurry, food production waste and silage effluent to waterbodies.

An unpolluted river water in summer, with an oxygen level of around 9 ppm (100 % saturation) will have a healthy flora and fauna which will include a population of bacteria which abound in nature. The latter will be mainly aerobic and their numbers are limited by the absence of suitable food, that is, digestible organic matter.

When there is an uncontrolled discharge of organic material (sewage, milk, silage liquor, etc.) the constraining factor on the growth of the bacterial pollution is removed. There is an immediate abundance of food and, initially, a corresponding plenitude of the dissolved oxygen. Bacterial growth is promptly stimulated and the population increases rapidly, consuming the available oxygen as it does so.

The growth of bacteria tends, therefore, to reduce the amount of oxygen dissolved in the water. The extent of oxygen depletion which occurs depends on the rapidity with which the stream takes up oxygen from the atmosphere, i.e. its re-aeration capacity. This capacity is greatest in fast-flowing, turbulent streams and least in deep, slow-flowing rivers. In addition, the loss of oxygen may be counteracted by the photosynthesis of green plants, which produce oxygen during daylight.

Where the degree of pollution is severe these compensating factors may be insufficient to prevent the oxygen content of the water decreasing to very low levels, or in the worst case, to anaerobic conditions, where there is a complete absence of free oxygen.

Deoxygenation is the most important potential effect of organic waste discharges.

The key to the resolution of water problems is *control*, by water quality management planning, by the enforcement of national and EU standards, by the licensing and policing of discharges, by following approved procedures in agriculture, and by good environmental awareness on the part of the public.

Finally, it is clear that monitoring dissolved oxygen is essential to control water quality and then life in water.

1.6 Oceans and seas

The mixing properties of the oceans unlike those of lakes, operate on a global scale, and supply oxygen to all ocean depths, including the deepest trenches, so that oxygen is rarely a limiting factor. This is not to say that oxygen is uniformly distributed, There is, for example, an oxygen minimum layer at about 400 to 1000 meters. Enclosed seas such as the Mediterranean may experience deoxygenation at times, as may the Norwegian fjords. The Black Sea, cut off from the Mediterranean by the Bosphorus, is permanently stagnant below 200 m, and therefore devoid of animal life, although anaerobic bacteria flourish.

1.7 An environmental monitoring sensor

In water or in air, the amount of dissolved oxygen is a vital parameter that has to be monitored. It is important for pollution control engineers to have a continuous record of dissolved oxygen levels in rivers, lakes, and reservoirs. Oceans are not in danger of gross pollution but there are many projects being suggested which involve the oceans as dumping grounds for the waste of modern day society. The goal of this project is to make an inexpensive and robust optical dissolved oxygen sensor. It will be used for the routine and long term monitoring of major rivers and lakes in Ireland, as well as coastal waters in the vicinity of industrial and sewage outfalls and sites of intensive aquaculture. This sensor will provide continuous time series data, which is often the only way to observe episodic events such as pollutants release which can lead to fish kills and lethal falls in dissolved oxygen.

The design of this sensor is introduced in Chapter 2. Current DO measurement technology is also discussed and the advantages of the optical technique highlighted. Subsequent chapters describe prototype design and testing and aspects of materials fabrication and optimisation.

References:

[1] Michael L. Hitchman, **"Measurement of Dissolved Oxygen"**, Ed. John Wiley & Sons, 1978.

[2] Gerard Kiely, **"Environmental Engineering"**, Ed. Irwin/McGraw-Hill, England, 1997.

[3] Enfo, **"Environmental Information Service"**, briefing sheet 11, April 98.

Chapter 2: Dissolved oxygen monitoring

2.1 Introduction

A sensor is a device capable of continuously and reversibly recording a physical parameter of the concentration of a chemical or biochemical species. *Wolfbeis.*

Two major techniques are currently employed to measure dissolved oxygen:

- The Winkler method [1,2] is the oldest standard method. Since 1988 it has been improved and is still the basis for the majority of titrimetric analyses.
- The electrochemical method, which was first developed by L. C. Clark in 1959 [2,3], is based on the reduction of oxygen at the cathode.

These techniques are described in this chapter.

2.2 The Winkler method

The method is based on the quantitative oxidation of Mn(II) to Mn(III) in alkaline solution with the subsequent oxidation of I^- by the Mn(III) in acid solution. The iodine, which is liberated, is titrated with thiosulphate in the normal way. The equations for the various steps are:

$$Mn^{2+} + 2OH^- \rightarrow Mn(OH)_2 \downarrow \quad [2.1]$$

$$2Mn(OH)_2 + ½\ O2 + H_2O \rightarrow 2Mn(OH)_3 \quad [2.2]$$

$$2Mn(OH)_3 + 6H^+ + 3I^- \rightarrow 2Mn^{2+} + I_3^- + 6H_2O \quad [2.3]$$

$$I_3^- \rightarrow I_2 + I^- \quad [2.4]$$

$$I_2 + 2S_2O_3^{2-} \rightarrow 2I^- + S_4O_6^{2-} \quad [2.5]$$

The method depends on the careful control of pH and I^- concentration and failure to do this can lead to significant errors [4,5]. Moreover, in any method for dissolved oxygen analysis which involves taking a sample of the water it is essential that atmospheric oxygen is not entrained or dissolved in the sample. Though this

laboratory method gives a very high precision it is not very efficient for DO monitoring in-situ due to the particular care in the collection of the samples.

2.3 The Clark electrode method

The system consists of a two-electrode cell with a membrane separating the electrodes and electrolyte solution from the test solution and, at the same time, keeping a thin layer of electrolyte in direct contact with the cathode. Oxygen from the test solution enters the membrane and diffuses through it into the film of electrolyte solution over the cathode. The dissolved gas diffuses across this layer to the cathode surface where it is reduced:

$$O_2 + 2H_2O + 4\,e^- \rightarrow 4\,OH^- \qquad [2.6]$$

The cathode is at such a negative potential that it reduces all the oxygen reaching its surface. The oxygen flux generated depends on the membrane characteristics and is proportional to the partial pressure of oxygen outside the membrane. Due to the reduction reaction, the electrical current generated between the two electrodes is proportional to this oxygen flux.

Electrochemical sensors based on the Clark electrode provide a convenient tool for oxygen determination. Though they are widely used, the drift of these sensors prevents their use for long term accurate measurements as they suffer from major drawbacks:

- The oxygen consumption renders the method unsuitable for use in very still water or in low oxygen concentration waters, as the oxygen could be underestimated.

- For in situ measurements, changes in the electrolyte composition could lead to erroneous results unless frequent calibration checks are made. Cells have limited lifetime and their replacement is expensive.

- When the diffusion properties of the membrane are altered (biofouling occurs, for example, during a few days usage) measurements tend to drift and become unreliable. To obtain quality measurements the membrane has to be regularly cleaned and the sensor has to be regularly calibrated, which makes this kind of sensor unsuitable for long term monitoring applications.

These problems can be theoretically overcome if optical sensing is used.

2.4 The optical method

Several optical methods are available to measure oxygen [6], but the determination of dissolved or gaseous oxygen is mainly based on the quenching of the fluorescence of an oxygen-sensitive dye by molecular oxygen [7,8,9,10]. Typically, the dye is incorporated into a gas-permeable membrane, and the fluorescence intensity or the fluorescence decay time, which are both dependent on the oxygen concentration, are determined [6].

Optical oxygen sensors have a number of advantages over current Clark electrode technology:

- They do not consume oxygen.
- Their ease of miniaturisation allows the development of very small, light, flexible and portable sensors.
- Analyses can be performed in real-time since no sampling is necessary.
- They have fast response times, which can be lower than with electrochemical sensors.
- Distributed sensing can be used via optical fibres.

- Optical sensors are simple in design and depending on the accessories, it is inexpensive to replace or substitute components, thus offering the possibility of disposable sensors.

- In comparison to electrodes where the membrane could be damaged without adequate pressure compensation, optical oxygen sensors can be subjected to high pressure.

The major disadvantages that optical sensors can exhibit will be discussed and studied in this thesis:

- Ambient light interferences, which will be investigated by using a black rubber silicone coating (Cf. Section 6.4).

- Long term stability, which is correlated to long term stability of the thin film matrix. For this purpose leaching of the film will be investigated (Cf. Section 6.2).

In spite of the large body of work published on optical oxygen sensors, there are only a few optical oxygen sensors commercially available, which makes the aim of this thesis even more interesting and challenging.

2.5 Context of the project

The development of optical dissolved oxygen sensors has been ongoing in this research group for the last five years. Sol-gel-based thin films, doped with the oxygen-sensitive Ru(diphenylphenanthroline) dye, have been developed, [11,12,13,14]. Also a laboratory-based sensor head, based on a Light Emitting Diode (LED) excitation, has been designed. Initial materials development and optimisation were carried out previously as part of another project [11]. While some progress toward a commercial sensor was achieved in a subsequent project [14], my project sets out to develop a prototype instrument for tests in the field. Some progress was

made toward temperature compensation and some material issues were addressed and improvements made. During the course of this project, the limitations associated with the intensity-based approach to optical sensing were identified. These will be discussed in subsequent chapters. Finally in chapter 9 the limitation of the design used in this project will be discussed in the light of an alternative improved apparatus now being implemented.

2.6 Objectives of the project

- To design and build a compact optical dissolved oxygen sensor which is capable of operation in the marine environment.

- To characterise and test the sensor under laboratory conditions.

- To test the sensor in a pressure vessel in collaboration with Seasense (company based in Galway).

- To perform field test also in collaboration with Seasense.

References:

[1] L. W. Winkler, **"The determination of dissolved oxygen in water"**, Berlin. Deut. Chem. Ges., 21: 2843 (1888).

[2] Michael L. Hitchman, **"Measurement of dissolved oxygen"**, Ed. John Wiley & Sons, New-York, 1978.

[3] L. C. Clark, **"Electrochemical device for chemical analysis"**, U.S. Patent 2, 913, 386, issued Nov. 17, (1959).

[4] G. Alsterberg, **"Methods for the determination of elementary oxygen dissolved in water in the presence of nitrite"**, Biochem. Z., **159**, 36 (1925).

[5] M. M. Jones and M. W. Mullen, **"Some aspects of the Winkler determination of oxygen in water"**, Talanta, **20**, 327 (1973).

[6] Otto S. Wolfbeis **"Fiber optic Chemical sensors and Biosensors"**, Vols.I & II, CRC Press, Boca Raton, Fl, 1991.

[7] I. Bergman, **"Rapid response atmospheric oxygen monitor based on fluorescence quenching"**, Nature (London), 218, 396, 1968.

[8] Wolfgang Trettnak, W. Gruber, F. Reininger and I. Klimant, **"Recent progress in optical oxygen sensor instrumentation"**, Sensors and Actuators B-CHEMICAL 29: (1-3) 219-225 Oct 1995.

[9] Chuang H and Arnold MA, **"Linear calibration function for optical oxygen sensors based on quenching of ruthenium fluorescence"**, Analytica Chimica Acta, 368: (1-2) 83-89 Jul 1998.

[10] S. McCulloch and D Uttamchandani, **"Fibre optic micro-optrode for dissolved oxygen measurements"**, IEE Proceedings-Science Measurement and Technology 146: (3) 123-127 May 1999.

[11] A.K. McEvoy, C.M. McDonagh, B.D. MacCraith, **"Dissolved oxygen sensor based on fluorescence quenching of oxygen-sensitive Ruthenium complexes immobilized in sol-gel-derived porous silica coatings",** Analyst, June 1996, Vol. 121 (785-788).

[12] B.D. MacCraith, C.M. McDonagh, G. O'Keeffe, A.K. McEvoy, T. Butler, F.R. Sheridan, **"Sol-gel coatings for optical chemical sensors and biosensors"**, Sensors and Actuators, B 29 (1995) 51-57.

[13] P.Lavin, C.M. McDonagh, B.D. MacCraith, **"Optimisation of Ormosil films for optical sensor applications"**, Journal of Sol-gel Science and Technology 13, 641-645, 1998.

[14] C.M. McDonagh, A.M. Shields, A.K. McEvoy, B.D. MacCraith, J.F. Gouin, **"Optical sol-gel-based dissolved oxygen sensor: progress towards a commercial instrument"**, Journal of Sol-Gel Science and Technology, Vol. 13, pp. 207-211, 1998.

Chapter 3: Optical method

3.1 Introduction

This chapter discusses the different physical principles involved throughout this work. The optical sensor is based on the fluorescence quenching of a ruthenium complex, which involves concepts like fluorescence, quenching of this fluorescence by oxygen and Stern-Volmer theory.

3.2 Fluorescence

Fluorescence is part of the large luminescence phenomenon [1], which includes all the phenomena where light is emitted by matter. Figure 3.1 shows the different steps involved in the process.

The *absorption process* is the excitation of a molecule or an atom from a ground state energy level to a higher energy level. The excited molecule is then subjected to collisions with the surrounding molecules, and as it gives up energy it steps down the ladder of vibrational levels (*non-radiative decay process*), to the lowest vibrational level of the excited electronic state. The de-excitation of the molecule to the ground state resulting in the emission of a photon of light is called fluorescence or phosphorescence. Usually, the ground state S_0 is a singlet state where electrons with opposite spins are paired. Depending on the spin orientation of its electrons, the excited state can be singlet or triplet (with electrons with the same spin orientation). If the excited state is a singlet state, then the radiative transition to the singlet ground state is called *fluorescence* and is short-lived (i.e. transition from energy level E_2 to E_0). If the excited state is a triplet state, then the radiative transition to the singlet ground state has low probability (it is spin-forbidden) and the emission may continue long after the original excited state was formed. This transition is called *phosphorescence*, (i.e. transition from energy level E_1 to E_0).

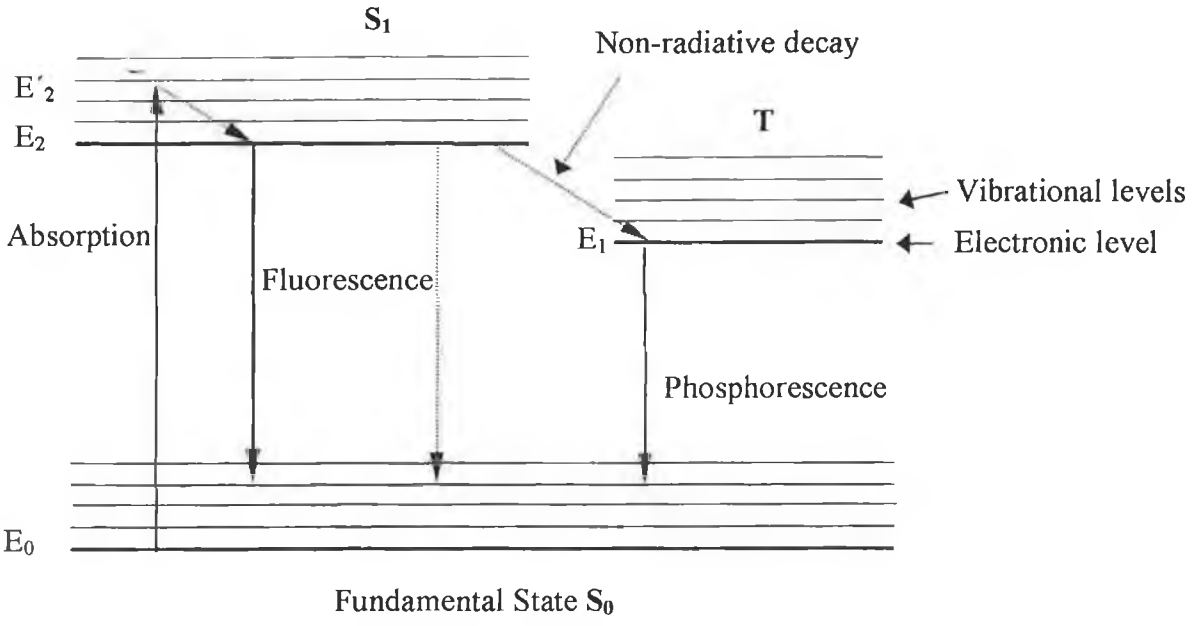

Figure 3.1: Simplified representation of photoluminescence phenomena.

The fluorescence properties can be affected by the environment. An increase of the temperature, causing an increase of the molecular agitation, favours intermolecular collisions and thus implies a decrease of fluorescence intensity and lifetime (defined below). The effect of concentration on fluorescence is complex. The number of emitted photons, and thus the fluorescence intensity is increasing with the number of molecules. Nevertheless, the collision probability between those molecules is increasing too. Finally, there is a compromise between both effects where fluorescence is maximum.

- **Fluorescence lifetime:**

After excitation of the sensor with a short light pulse, the duration of the emission, by definition the time it takes for the intensity to achieve 1/e of its original amount, is called the fluorescence lifetime τ (Cf. Figure 3.2). The observed lifetime depends on both the radiative and non-radiative decay rates as given by equation 3.1.

$$K_{obs} = \frac{1}{\tau_{obs}} = \frac{1}{\tau_{rad}} + \frac{1}{\tau_{non-rad}} \qquad [3.1]$$

With: K: decay rate

τ_{obs}, τ_{rad}, $\tau_{non\text{-}rad}$: observed, radiative and non radiative lifetimes respectively.

Note that the process of oxygen quenching (discussed later in this chapter) involves a reduction in observed lifetime due to the increased non-radiative decay.

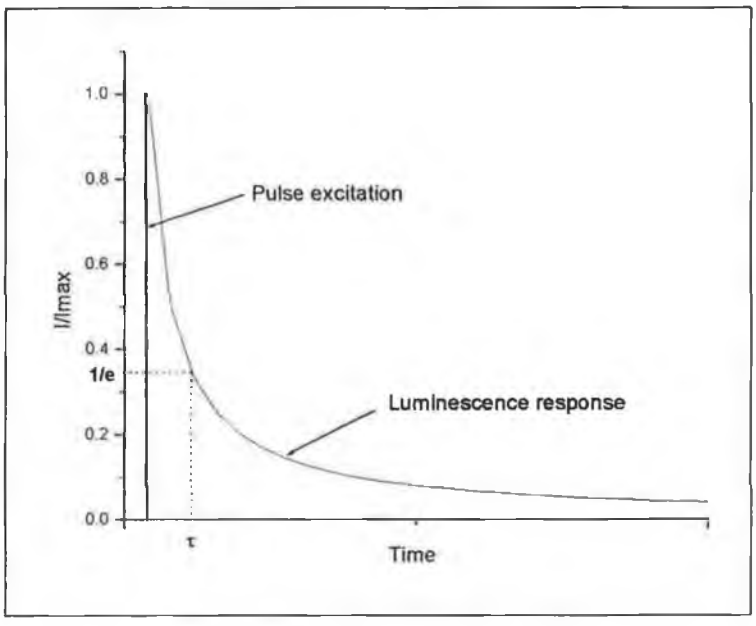

Figure 3.2: Characteristic fluorescence lifetime curve after pulse excitation.

Two techniques are available to determine this luminescence lifetime. The direct method (time domain) which evaluates the decay profile of the monitored lifetime, and the indirect method (frequency domain) which uses the time delay (phase shift) of a sinusoidally modulated luminescence signal.

3.3 The fluorophore: the ruthenium complex

The use of fluorescent transition metal complexes in the development of fluorescent optical sensing devices has become increasingly widespread due to their desirable characteristics. These compounds tend to be thermally, chemically, and photochemically stable, resulting in long term stability and durability of the sensors. They exhibit strong absorption in the blue-green region of the spectrum ensuring compatibility with a large range of suitable excitation light sources. For transition metal complexes, the Stokes shift, which is the wavelength difference between absorption and fluorescence maxima, is relatively large and enables easy differentiation between excitation and emission light (Cf. Figure 3.3).

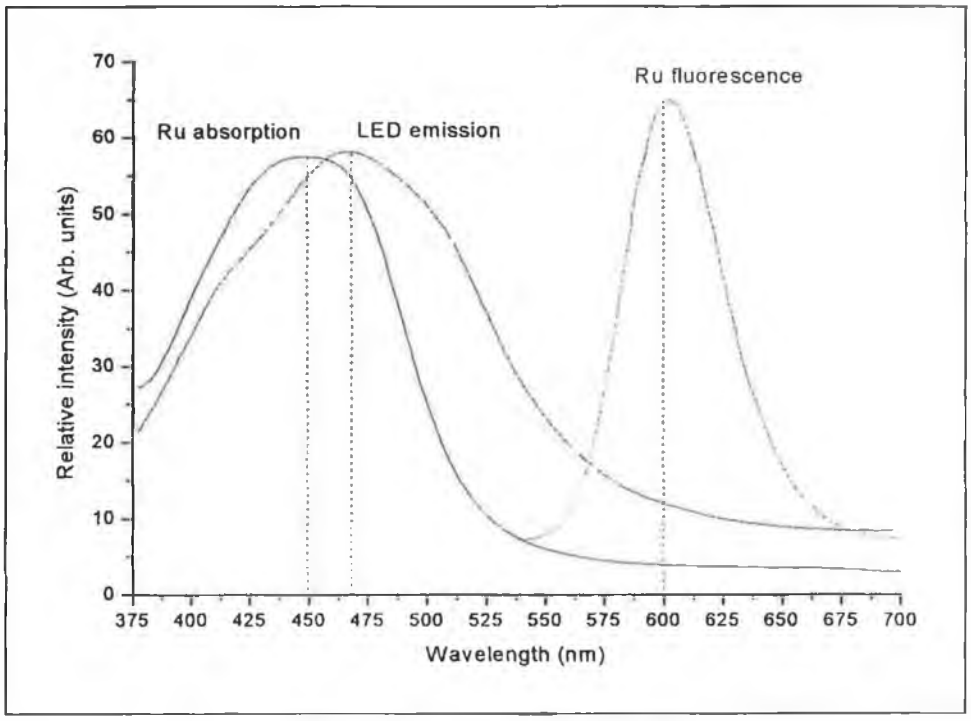

Figure 3.3: Emission spectrum of the LED and ruthenium complex absorption and fluorescence.

The ruthenium complex (Cf. Figure 3.4), [Ru(II)-tris(4,7-diphenyl-1,10-phenanthroline)]$^{2+}$ written [Ru(Ph_2phen)$_3$]$^{2+}$ was the dye chosen as it exhibits a high oxygen sensitivity and has a long fluorescence lifetime ($\tau_o \approx 5\mu s$ in absence of oxygen) [2].

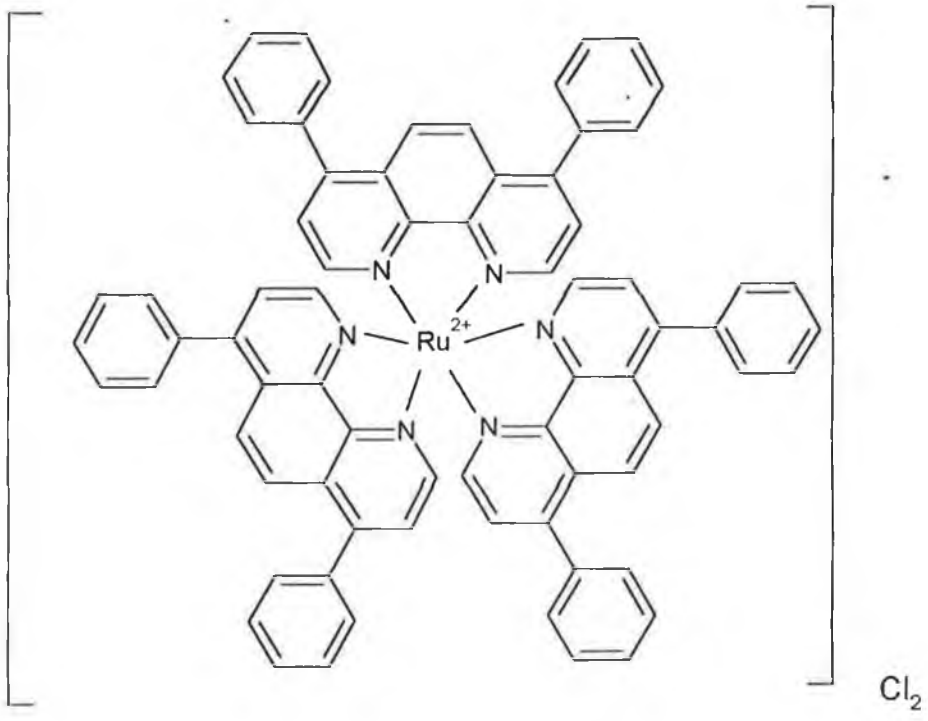

Figure 3.4: Tris-(4,7-diphenyl)-1,10-phenanthroline ruthenium(II) Chloride, known as ruthenium complex.

The chemical structure of this compound consists of the ligand (Ph_2phen) attached to the ruthenium atom via nitrogen atoms (N). Each ruthenium atom is surrounded by three ligands. The ruthenium complex has partially filled d^6 orbitals, the ordering and occupancy of which determines the emissive properties [2]. The octahedral field of the ligand splits the five degenerate orbitals resulting in a triply degenerate t_{2g} level and a doubly degenerate e_g level. The magnitude of the energy difference is the crystal field splitting, Δg (Cf. Figure 3.5).

The ligands have π and σ orbitals, but only the π orbitals are significant for visible and near-UV absorptions and emissions. There are both π bonding (π) and π antibonding (π^*) levels in which only the π bonding levels are filled.

The excitation of the complex results in the elevation of an electron to one of three possible excited states:

(1) A d electron is promoted to another d level, i.e. a d-d transition.

(2) A π bonding orbital electron is promoted to a π* antibonding orbital, i.e. a π-π* transition.

(3) (a) A d electron is promoted to a π* antibonding orbital, known as Metal to Ligand Charge Transfer state (MLCT state).

(b) A π bonding orbital electron is promoted to an unfilled d orbital, known as Ligand to Metal Charge Transfer state (LMCT state).

The MLCT transition is the lowest in energy with respect to all other possible excited state transitions. Consequently this state is primarily responsible for the absorption and emission characteristics of the complex.

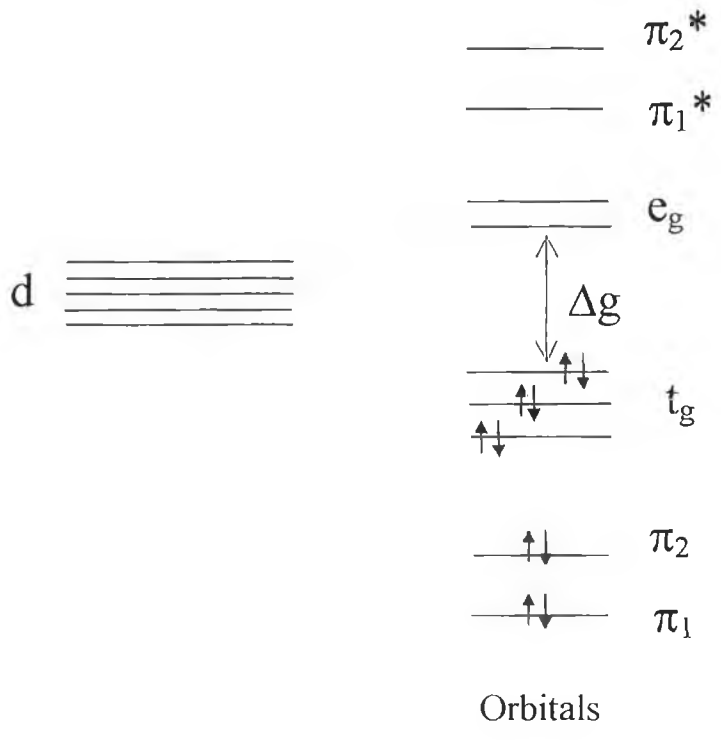

Figure 3.5: Simplified orbital diagram for Ru(II)-tris(4,7-diphenyl-1,10-phenanthroline).

The $[Ru(Ph_2phen)_3]^{2+}$ has an absorption maximum at 450 nm and the Stokes-shifted emission of the MLCT excited state to the ground state results in a fluorescence maximum at 609 nm in sol-gel films, when excited by a blue LED (Light Emitting Diode, λ_{max} = 476 nm) as shown in Figure 3.3.

3.4. Fluorescence quenching by oxygen

3.4.1 Introduction

Fluorescence quenching results in the decrease of fluorescence intensity of a given substance and can take the form of either static or dynamic quenching.

• The *static quenching* occurs as a result of the formation of a non-fluorescent complex between the fluorophore (at a non-excited state) and the quencher. When this complex absorbs light it immediately returns to the ground state without the emission of a photon.

Static quenching: $F + Q \rightarrow FQ$ [3.2]

• The *dynamic quenching* results from collisional encounters between the fluorophore and the quencher. The quencher diffuses to the fluorophore during the lifetime of the excited state. Upon contact, the fluorophore returns to the ground state without the emission of a photon. The quenching is dependent on the concentration of the quenching molecule and on the rate at which the quencher can diffuse to the excited fluorophore.

In this work, the fluorescence quenching is due to dynamic quenching by molecular oxygen.
The complete process can finally be summarised by the following equations:

Absorption:	$Ru + h\nu \rightarrow Ru^*$	[3.3]
Fluorescence:	$Ru^* \rightarrow Ru + h\nu$	[3.4]
Non-radiative transition	$Ru^* \rightarrow Ru$	[3.5]
Quenching	$Ru^* + O_2 \rightarrow Ru + O_2^*$	[3.6]

Where the suffix * corresponds to the excited state, and hν symbolises a photon.

3.4.2 The Stern-Volmer equation

As the quenching affects both the intensity and the lifetime of the fluorophore, collisional quenching of fluorescence can be described by the following Stern-Volmer equations [3]:

$$\frac{I_0}{I} = 1 + k\tau_0[O_2] \qquad [3.7]$$

$$\frac{\tau_0}{\tau} = 1 + k\tau_0[O_2] \qquad [3.8]$$

With: I_0 and I: fluorescence intensities in absence and presence of oxygen.

τ_0 and τ: lifetime of the Ru in absence and presence of oxygen.

$[O_2]$: dissolved oxygen concentration.

k: bimolecular quenching constant defined as $k \propto D\alpha$

where α is the oxygen solubility in the matrix and D the diffusion coefficient of oxygen in the sensing film.

K_{SV} is the Stern-Volmer constant, which is given by:

$$K_{SV} = k\tau_0 \qquad [3.9]$$

The equations [3.7] and [3.8] can therefore be written like:

$$\frac{I_0}{I} = 1 + K_{SV}[O_2] \qquad [3.10]$$

$$\frac{\tau_0}{\tau} = 1 + K_{SV}[O_2] \qquad [3.11]$$

These relationships can be expressed as straight lines with intercept of 1 on the y-axis and slope K_{SV} as shown in Figure 3.6.

The sensor can be based on monitoring either the intensity or the lifetime.

3.4.3 The fluorescence quenching experiment

The fluorescence quenching of the Ruthenium dye by oxygen is determined by measuring the fluorescence intensity I as a function of oxygen concentration $[O_2]$. Prior to measuring the quenching response of a film, the baseline level (or offset) must be determined in order to be aware of the background level. It is done by running the system with a blank (non-coated) glass slide, while flowing deionised water through the sensor cell described in Chapter 5.

The method to characterize the quenching response of a particular film is to measure the fluorescence intensity of fully deoxygenated water (100 % Nitrogen) and fully oxygenated water (100 % Oxygen). The quenching value of the film can be calculated from this data using the following equation:

$$Q = \frac{I_{N_2} - I_{O_2}}{I_{N_2} - I_b} \qquad [3.12]$$

With: Q : Quenching coefficient.

I_{N2} : Fluorescence intensity with 100 % nitrogen or 0% oxygen.

I_{O2}: Fluorescence intensity with 100 % oxygen.

I_b : Baseline intensity, .

Different notations like Q_b or Q_a are found in the thesis. They stand for the quenching values calculated with the baseline intensity measured before (Q_b) or after (Q_a) the measurement. This baseline intensity was the offset of the measurement and was usually fixed at about 0.4V in order to be aware of any fluctuation in the LED intensity.

3.4.4 Ksv calculation/plots

The Stern-Volmer graph is plotted using equation [3.10], by flowing different levels of oxygenated water in the range of 0 % to 100 % and monitoring the intensity I.
For all the different measurements taken, the Stern-Volmer plots obtained were linear, a typical example is shown in Figure 3.6.

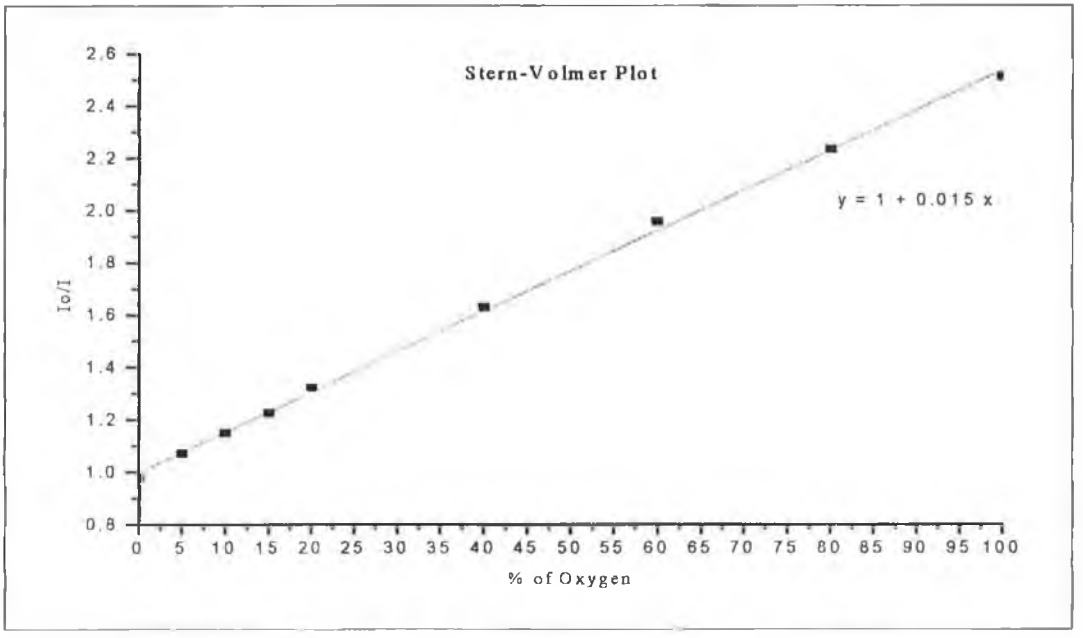

Figure 3.6: Stern-Volmer plot from 0 to 100 % oxygen.

Assuming this linearity [4,5], to plot equation [3.10], instead of taking I_0, as the measured point for deoxygenated water (or 0 % oxygen), I_0 has been calculated from a linear regression program from all the points together from 1/I plot. This has been found to give more consistent values of K_{sv} than taking the measured value of I_0.

3.5 Summary

This chapter introduced the optical concepts involved in the oxygen sensor. The fluorophore used is the diphenylphenanthroline ruthenium complex written $[Ru(Ph_2phen)_3]Cl_2$ or Ru(dpp), and the technique is based on its fluorescence intensity, which is quenched by oxygen.

References

[1] **"Practical Fluorescence, Theory, Methods and Techniques"**, by George G. Guibault, Marcel Dekker, Inc., NY, 1973.

[2] J.R. Bacon and J.N. Demas, **"Determination of oxygen concentrations by luminescence quenching of a polymer-immobilized transition-metal complex"**, Anal. Chem., 59 (1987) 2780-2785.

[3] O. Stern and M. Volmer, Z. Physics, 1919, Vol.. 20, pp183.

[4] Watkins AN, Wenner BR, Jordan JD, Xu WY, Demas JN, Bright FV, **"Portable, low-cost, solid-state luminescence-based O2 sensor"**, Applied Spectroscopy, 52: (5) 750-754, May 1998.

[5] J. F. Gouin, F. Baros, J. C. Andre, **"A fiber optic oxygen sensor for oceanography"**, Ifremer Brest, 1996.

Chapter 4: The sol-gel process and thin film fabrication

4.1 Introduction

A *sol* is a colloidal suspension of solid particles in a liquid.
A *gel* is an interconnected rigid network with pores of submicrometer dimensions and polymeric chains whose average length is greater than one micron [1].
The *sol-gel* fabrication involves the formation of an interconnected three-dimension network of Si-O-Si molecules produced by the simultaneous hydrolysis and polycondensation of a metal alkoxide. This metal alkoxide is also known as a precursor and consists of a metal element surrounded by various ligands. The metal alkoxide used in this project was methyltriethoxysilane (MTEOS, $CH_3(C_2H_5O)_3Si$), which has the advantage of increasing the hydrophobicity of the film as discussed in Section 4.3.

4.2. The sol-gel process

4.2.1 Hydrolysis and condensation

The first step in the sol-gel process is hydrolysis (Cf. Equation 4.1). The silicon alkoxide precursor is hydrolysed by mixing with water. The hydrolysis involves the nucleophilic attack by the oxygen in water on the silicon atom, resulting in the replacement of the alkoxide groups OR (where R is an alkyl group C_XH_{2X+1}), with the hydroxyl groups OH.

$$\equiv Si - OR + H_2O \leftrightarrow \equiv Si - OH + ROH \qquad [4.1]$$

This is followed by condensation. The condensation reactions (Cf. Equations 4.2 and 4.3) involving the silanol groups, Si - OH, occur via a nucleophilic condensation

reaction and produce siloxane bonds Si - O - Si, along with by-products of alcohol ROH or water.

Alcohol condensation: $\equiv Si - OR + HO - Si \equiv \Leftrightarrow \equiv Si - O - Si \equiv + ROH$ [4.2]

Water condensation: $\equiv Si - OH + HO - Si \equiv \Leftrightarrow \equiv Si - O - Si \equiv + H_2O$ [4.3]

These reactions often begin before the hydrolysis reaction is completed.

4.2.2 Gelation

The alcohol itself is an important component in the sol-gel process as it participates in the reverse reactions shown in equations 4.1 and 4.2. In the sol-gel process, the condensation reactions continue to build up long polymeric chains of Si-O-Si molecules which, with time, interlink to become a three-dimensional network known as a gel.

The physical characteristics of this gel network depend upon the size of particles and extend of cross-linking prior to gelation. The sol becomes a gel when it can support a stress elastically. This is defined as the gelation point or gelation time t_g. Experimentally, the point of gelation is marked by a sharp increase in the viscosity of the sample due to an increased number of interconnected particles.

4.2.3 Aging and drying

Aging is the term used to describe the process whereby after the ingredients have been mixed the sol is left at room or elevated temperature to accelerate the hydrolysis and condensation process. The main function of aging is to increase the viscosity of the solution to ensure that dip-coating is possible (Cf. Section 4.3).

After dip-coating the sol onto the substrate, the glass slides were placed into an oven at 70°C for 18 hours. This is known as the drying time, which serves to remove excess liquid from the interconnected pore network [2].

4.3. Sol-gel processing parameters

4.3.1 Choice of precursor

The most common precursor used in sol-gel work is TEOS (tetraethoxyorthosilane). In this work an organically modified or ormosil precursor was used, which produces a more hydrophobic film surface with less adsorbed water compared to TEOS films. The chosen precursor was MTEOS (methyltriethoxysilane). It has been established that the operation of the dissolved oxygen sensor used for this work is based on the principle whereby the oxygen partitions out of the water at the film/water interface and accesses the ruthenium dye in gas phase. The hydrophobic nature of the ormosil films is clearly conducive to this partitioning effect [3,4].

4.3.2 Influence of R (molar ratio of Water to Precursor)

An important parameter in the sol-gel process is R, molar ratio of water to silicon alkoxide precursor, as water is used in the hydrolysis reaction and evolved in the condensation reaction (Cf. Section 4.2.1). Therefore, the amount added to the initial solution can strongly influence the structure of the resultant gel. Theoretically an R value of 2 is sufficient for complete hydrolysis and condensation to occur [2]. Generally, an increase of the R value decreases the gel time of a sol, providing a more viscous sol which will in turn produce a thicker film. For this work it has been found that the ratio R = 4 produces the optimum films [3,5].

4.3.3 Influence of pH

The rates of both hydrolysis and condensation reactions are dependent upon the pH of the starting solution. The isoelectric point of silica, at which the electron mobility and the surface charge is zero, occurs at pH=2. This pH value defines the boundary between acid catalysis (pH<2) and base catalysis (pH>2) in the silica sol-gel process [2]. Acid catalysis results in fast hydrolysis rates and relatively long gel times. The

resulting gel consists of a network structure of linear chains with a fine microporous structure. Alternatively, base catalysis is associated with slow hydrolysis rates, faster condensation rates and hence faster gel times. Under these conditions, more dense colloidal particles are formed with larger pore sizes.

4.4 The substrate

For the most part, glass slides were used as a substrate for this study. To produce a durable, uniform and good quality thin film the substrate had to be cleaned prior to the dip-coating process. Glass substrates were prepared from microscope slides 1.00 mm thick, cut into pieces of 15 mm x 25 mm according to the sensor head prototype size. The glass slides were cleaned by washing with different chemicals as follow:

- deionised water
- methanol
- acetone
- deionised water

The glass slides were then immersed in deionised water and placed in an oven at 70°C for a night. This cleaning process is thought to condition the slides by increasing the number of surface silanol groups and hence improve adhesion of the sol-gel film to the substrate.

4.5 Dip-coating

Numerous deposition techniques exist to coat the film on the substrate including: spin-coating [6,7,8,9], dip-coating [6,8], spray-coating [10], knife-coating [8], drop-coating [7], stamp-coating [11] and screen printing [12]. The choice of the method depends mainly on the characteristics (for example viscosity) of the mixture and on the film thickness desired, as a perfect evenly coated surface is required. To obtain reproducible, identical and uniform films, the dip-coating technique appeared to be ideal, and was therefore used for this study. Moreover, the dip-coating method was chosen as it allows the deposition of thin layers of very precise thickness (Cf. Section 6.3). Some drop-coating films have been made for a separate study (Cf. Chapter 6).

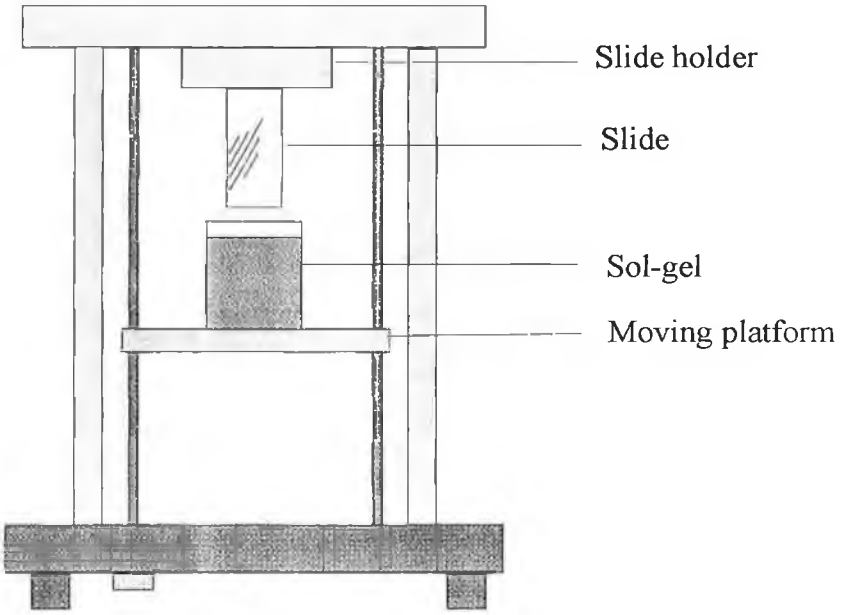

Figure 4.2: Dip coating apparatus.

Dip coating involves withdrawing a substrate vertically from a coating reservoir at a constant speed. The films made for this project were deposited using a computer controlled dip coating apparatus (Cf. Figure 4.2). The coating speed was for most films 0.99 mm/sec. For thickness studies different coating speeds were chosen, from 0.2 mm/sec to 3 mm/sec.

The dip-coater raises the platform with the sol reservoir to the substrate which is held above. When the substrate has been immersed, the platform is lowered depositing the film on the substrate. Dipping was carried out in a draught free and vibration free environment, but at ambient temperature, pressure and humidity.

4.6. Fabrication details

4.6.1 The procedure

The procedure used for making MTEOS R = 4 films was as follows:

Ruthenium:	0.0162 g
Ethanol:	4.1508 g
H_2O (pH=1):	1.0376 g
MTEOS:	2.5680 g

The ruthenium was first mixed and dissolved in ethanol. A solvent such as ethanol is usually required as a homogenising agent because water and silicon alkoxides are immiscible. After mixing the solution with water, MTEOS was added dropwise in the mixture. The ingredients were finally mixed for one hour with a magnetic stirrer in order to obtain a homogeneous solution. The hydrolysis and condensation reactions were left to proceed for a period known as the aging time. Consequently, the sol was viscous enough for further processing. Sensor films were then coated as described in Section 4.5. All the measurements have been taken with slides from the same batch of methyltriethoxysilane (MTEOS) R=4, single side coated made on the same day. Any comparison is reliable, as all of them should have the same behaviour as they are stored in the same way. Two slides have been used for 12 months, first with the prototype and then with the laboratory system. The slide labeled DW was stored in deionised water while all the others were stored in air.

4.6.2 Sensor dye incorporation

One advantage of the sol-gel technology is that the gas permeable solid matrix is a very suitable host for dye complexes, which are easily incorporated during the fabrication of the sol-gel without any damage to the complex. One of the only drawbacks of the immobilisation technique is that there is a certain amount of leaching out of the entrapped reagent from the matrix [13]. However, it is possible to overcome such problems by covalently binding the reagent to the matrix or employing matrices with extremely small pore dimensions. A balance in pore size is reached whereby any leaching of the dye is minimised but the dye remains accessible to the analyte via the pores. This is achieved by using low pH water (Cf. Section 4.3).

4.7 Conclusion

The sol-gel technique described in this chapter offers a low cost and versatile route for the production of thin porous glass films. The process is reliable, reproducible and gives good results when used with the dip-coating technique.

By varying parameters like pH, R (molar ratio of water to precursor) or dip-coated speed it is possible to vary film properties, like pore size or thickness of the film, and thus tailor the film microstructure for specific purposes.

References

[1] Hench L.L., West J.K., **"The sol-gel process"**, Chem. Rev., 1990, vol. 90, pp. 33-72.

[2] Brinkler C.J., Scherer G.W., **"Sol-gel Science"**, 1990, Academic Press, New York.

[3] A. K. McEvoy, **"Development of an optical Sol-Gel-Based Dissolved Oxygen Sensor"**, PhD thesis, Dublin City University, 1996.

[4] C. McDonagh, B. D. MacCraith and A.K. McEvoy, **"Tailoring of sol-gel films for optical sensing of oxygen in gas and aqueous phase"**, Anal. Chem. 1998, Vol. 70, pp 45-50.

[5] A. Doyle, **"Development of optical sensor platforms based on evanescent wave interactions"**, PhD thesis, Dublin City University, 1999.

[6] Scriven L.E., **"Physics and Applications of Dip-Coating and Spin-Coating"**, Better Ceramics through Chemistry III, 1998, Mat. Res. Soc., Pittsburgh, pp.717-729.

[7] Martin M.F. Choi, Dan Xiao, **"Oxygen-sensitive reverse-phase optode membrane using silica-adsorbed ruthenium(II) complex embedded in gelatin film."**, Analytica Chimica Acta, 387, 197-205, 1999.

[8] Ronnie Nohr Glud & Al., **"Planar optrodes: a new tool for fine scale measurements of two-dimensional O2 distribution in benthic communities"**, Marine Ecology Progress Series, Vol. 140:217-226, 1996.

[9] M. C. Matos, A.R. Carvalho and R.M. Almeida., **"Influence of processing parameters on the thickness of sol-gel silica films"**, Proc. SPIE, Vol. 1758, Ed. By J. O. Machenzie (Bellingham, Washington: SPIE), pp 77-82, 1996.

[10] C. Goebbert, R. Nonninger, M.A. Aegerter and H. Schmidt, **"Wet chemical deposition of ATO and ITO coatings using crystalline nanoparticles redispersable in solutions"**, Thin Solid Films, 351 (1999), pp 79-84.

[11] Conor Burke and Dr. A.K. McEvoy, personal communications, Optical Sensors Group, Dublin city University.

[12] Stephen A. Wring, **"Chemically Modified, Screen-printed Carbon Electrodes"**, Analytical Applications of Chemically Modified Electrodes, Bristol, UK, January 7-8, 1992.

[13] Butler T.M., MacCraith B.D., McDonagh C., **"Leaching in Sol-gel-Derived Silica Films for Optical pH Sensing"**, Journal of Non-Crystalline Solids, 1998, Vol. 224, pp. 249-258.

Chapter 5: Sensor characterisation instrumentation

5.1 Introduction

This chapter describes the sensor characterisation instrumentation used in the project. Both the laboratory-based system and the prototype system are discussed. The technique used for measuring film thickness is also explained.

5.2 The laboratory-based test system

As discussed in Chapter 2, the initial phase of the development of this sensor used a laboratory-based characterisation system. This system was also used in this project for references purposes with respect to the prototype sensor system.

The sensor characterisation instrumentation is shown in Figure 5.1. Water samples were prepared by flowing a gas mixture of nitrogen and oxygen from two mass flow controllers (Unit Instruments Ltd., Ireland) into a sealed flask of deionised water. The gas entered the water via an air stone diffuser (the same as used in an aquarium) in order to avoid big bubbles and facilitate the gas dissolution in water. Gas and water were mixed vigorously and continuously using a magnetic stirrer, in order to maintain gas saturation. The water sample was then flowed via a peristaltic pump (Gilson, France; Model Minipuls 3) to the water cell for measurement. All measurements were performed at ambient temperature, which means at non-constant temperatures. Temperature fluctuations were especially significant while comparing measurements done in winter or in summer. Measurements were also performed at constant flow.

Data from the sensor were digitised by a multifunction input/output board (Bytronics, West Midlands, U.K.; Model MPIBM3) and monitored by a PC for display and analysis using a Labview program. Note that all intensity and temperature data are monitored in voltage.

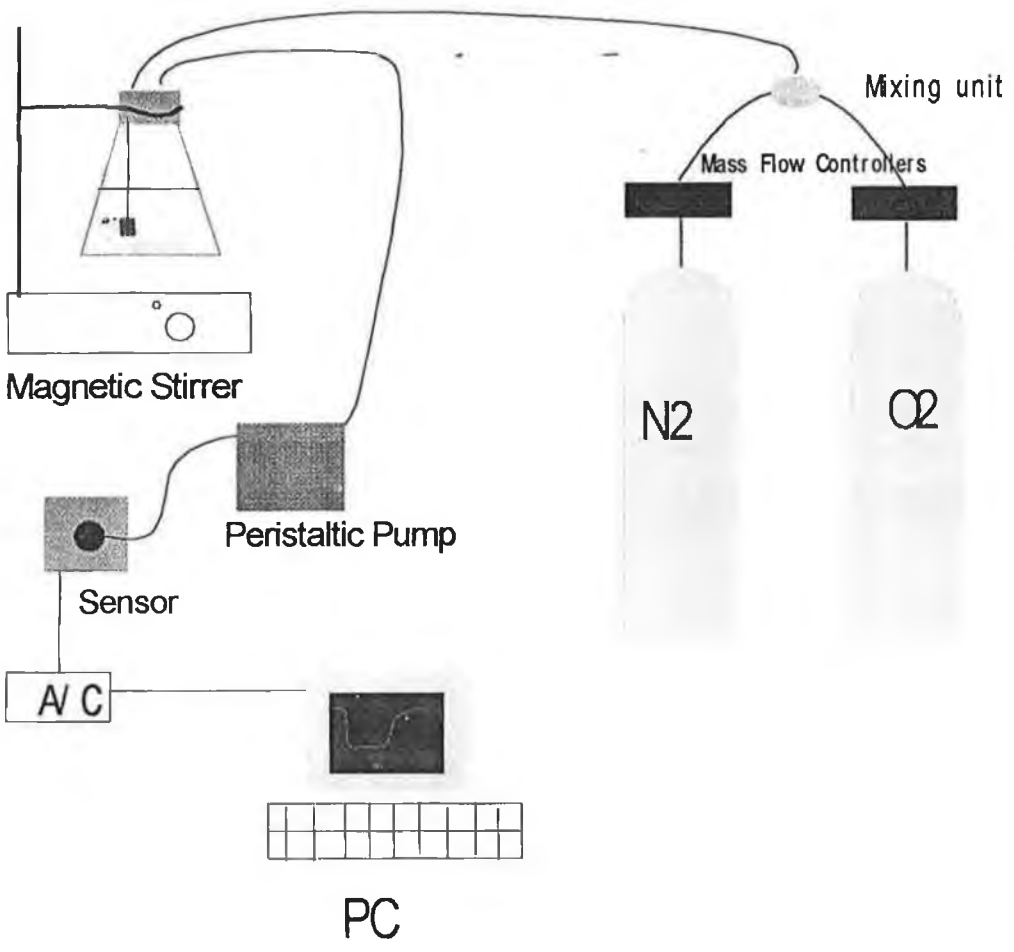

Figure 5.1: Experiment set-up.

The sensor cell is shown in Figure 5.2. The excitation source is a high intensity blue LED (Ledtronics, Torrance, CA) whose spectral output peaks at 450 nm. To prevent overlap between the LED excitation light and the fluorescence emission light, the light coming from the LED passes through a wide-band pass filter, 400 – 505 nm (Infrared Engineering, Maldon, Essex, U.K.). It is then focused onto a sol-gel coated glass slide, which is held at 45° to the excitation beam in a sealed cell. Fluorescence from the coated glass slide passes through a long-wave pass filter, $\lambda_{cut\text{-}on}$ = 570 nm, (CVI Laser Corporation, Albuquerque, N.M., U.S.A) and is focused onto a silicon photodiode detector (Hamamatsu, Middlesex, U.K.; Model S1223-01).

The sealed cell has inner dimensions of 15 mm x 15 mm x 40 mm giving an approximate volume of 9 cm^3.

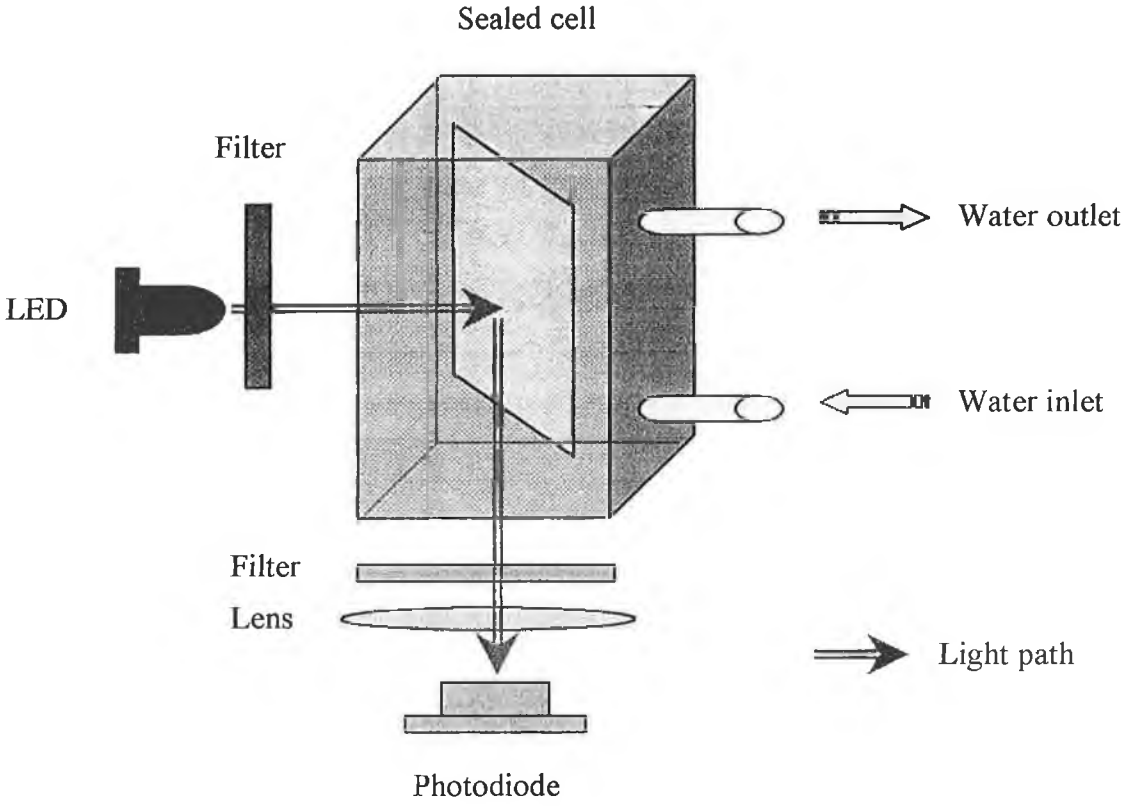

Figure 5.2: Laboratory system configuration.

5.3 The prototype sensor system

For most of this project a prototype sensor cell replaced the laboratory cell shown in Figure 5.2. One of the primary objectives of the sensor development was to build a configuration which could be immersed in water for testing.

- All elements of the sensor, except the sensing film, had to be encased in a water tight housing in a design as compact as possible.

- Another photodiode had to be added in order to monitor any fluctuations in the LED excitation light, which would influence the fluorescence intensity response signal.

- A problem of air pockets at the film/water interface led to a configuration where the sensing film was on the side of the sensor instead of the bottom or top of the sensor.

Figure 5.3 shows the head of the prototype sensor. Although the slide is shown mounted at the bottom, in practice the whole assembly was rotated by 90° such that the film was on the side. This minimised air bubble interferences. The prototype sealed flow cell is nearly three times bigger than the laboratory cell. Its inner dimensions are of 48 mm in diameter and 14 mm in height, which correspond to a volume of 25 cm^3. This flow cell was used for testing, in the laboratory. For field tests however, the probe will be immersed with the film in contact with the water.

To fix the glass slide on the O-ring (Cf. Figure 5.3 b), which sealed the sensor head, a circular piece of metal is screwed over the slide. This metal ring has special dimensions to prevent the slide from breaking and has two channels (on the glass side) in order to allow any undesirable gas bubble to leave and have a measurement free of its interference.

Unlike the laboratory system, which has only one output signal coming from the single photodiode, the prototype has a number of outputs:

- The photodiode, which is held at 45° to the glass slide, records the light passing through a blue filter, i.e. the light coming from the LED. This photodiode is called the reference photodiode.
  The signal recorded is called $\mathbf{I_{ref}}$.

- The photodiode, which is held directly above the glass slide, records the light passing through a red filter, i.e. the fluorescence light emitted. This photodiode is called the fluorescence photodiode.
  The signal is called $\mathbf{I_{fluo}}$ when recorded using a coated slide and $\mathbf{I_{baseline}}$ when recorded using a blank slide.

  As the fluorescence intensity is much lower than the LED intensity, the signal recording the fluorescence is amplified by 56 times more than the signal recording the emission light.

- Two sensors record the temperature: one inside the box, near the electronics for the temperature inside (Temp. inside), and another one outside the box, in the flow cell, for the temperature outside (Temp. outside). The calibration formula provided by the temperature sensor supplier is not accurate, so that the values recorded are only indicative.

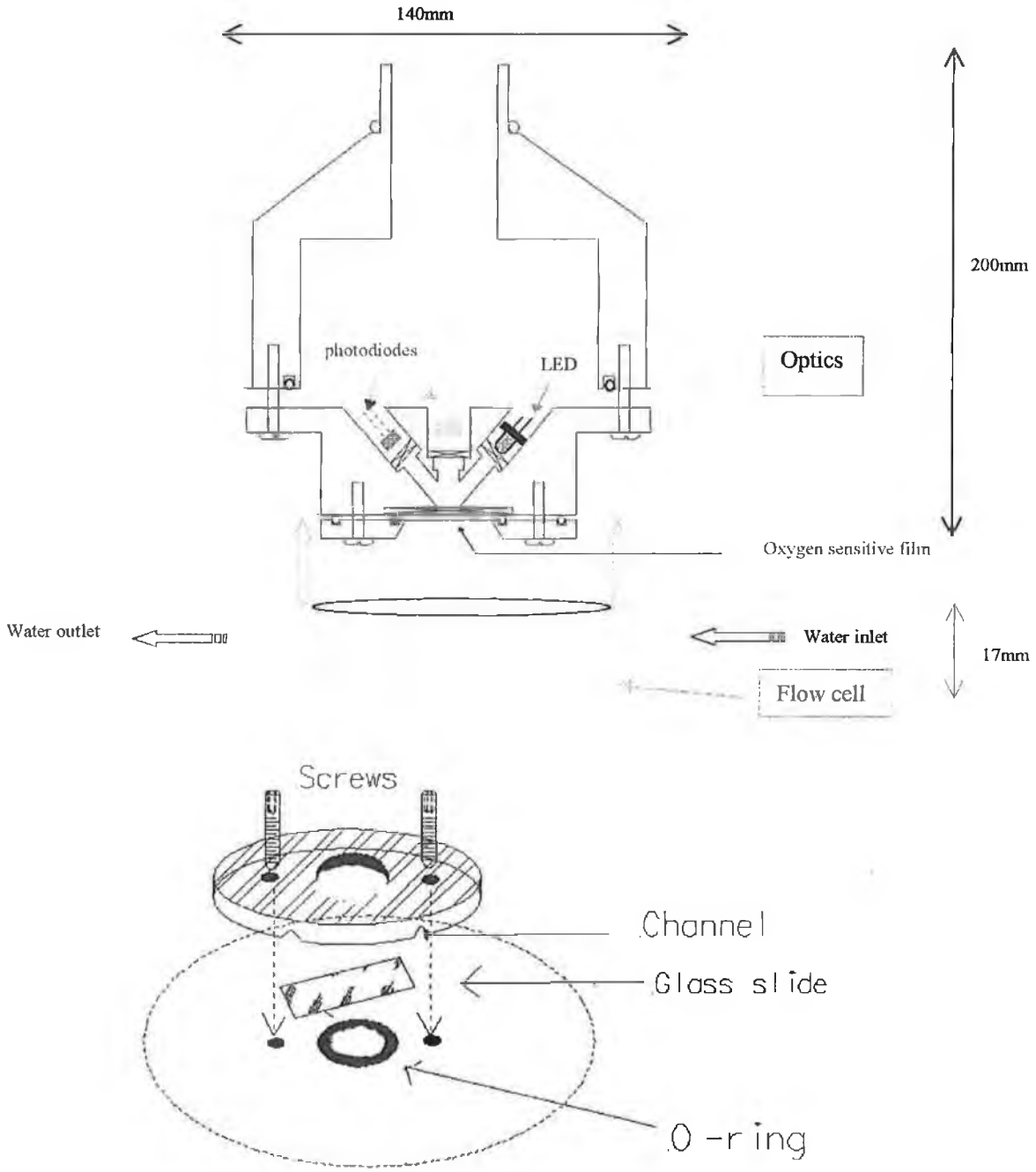

Figure 5.3 (a) and (b): Prototype sensor configuration.

5.3.1 Filters

Since background light from the LED could mask the require fluorescence signal, a careful choice of optical filters is important.

The filters are made by CVI Laser corporation (Albuquerque, USA). The blue one is 3mm thick and the orange one is 2mm thick. As shown in Fig. 5.4, the wavelengths between 530 nm and 670 nm pass through the orange filter, while the blue filter cuts the wavelengths higher than 540 nm.

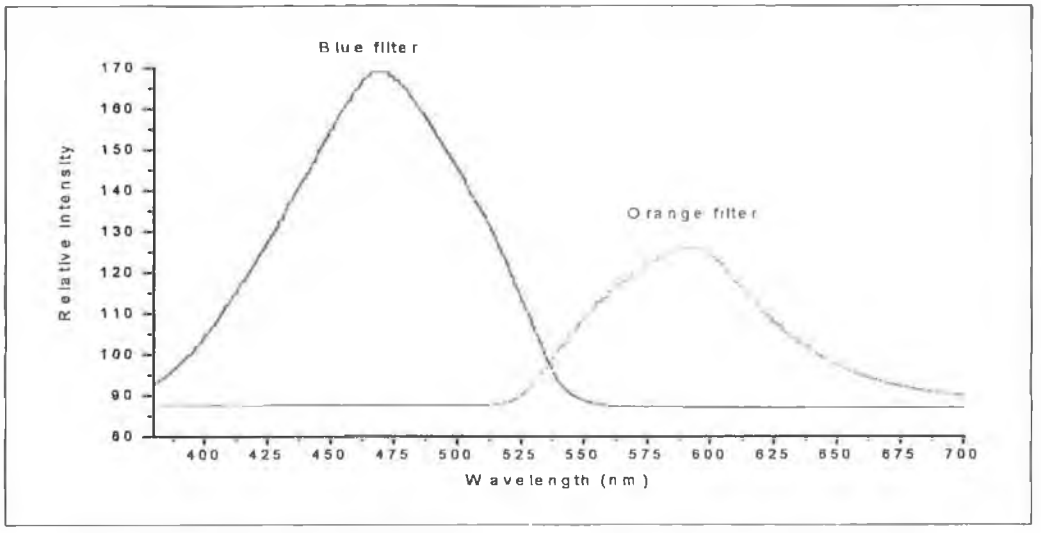

Figure 5.4: Light spectra passing through the blue filter and the orange filter.

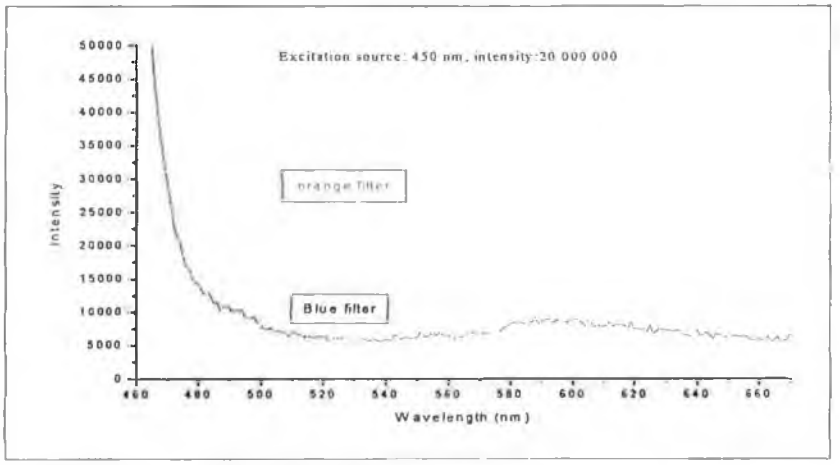

Figure 5.5: Fluorescence of the filters.

According to Figure 5.5, it seems that around 600 nm the orange filter has a tiny fluorescence, corresponding to 0.04 % of the excitation light intensity. This small amount of fluorescence will contribute a little to the background signal.

5.4 Measurement protocol

As both cells do not have the same configuration they do not behave identically and were then not used exactly in the same way.

In the laboratory system the signal was continuously monitored and the gas saturated water was continuously flowing in the sealed cell.

As seen in Chapter 3, a typical sensor response is the result of flowing gas saturated water with increased Oxygen/Nitrogen ratio from 0 to 100 % (i.e. from fully deoxygenated water to fully oxygenated water) through the cell. This means that while the ratio of Oxygen/Nitrogen was changed with the mass flow controller, the water was still flowing through the cell though the ratio was not obtained yet in the flask. The equilibrium in the cell was obtained fairly rapidly, and the resulting value was obtained after waiting for the response time delay due to the gas switch over. For a 0 % and 100 % oxygen test, the time delay to obtain the correct value was about 10 min for 100 % oxygen and about 20 min for 0% oxygen (i.e. 100 % nitrogen) after changing the gas ratio on the mass flow controller (Cf. Figure 5.6). This longer delay to reach the 100 % nitrogen level was due to the difficulty of removing the oxygen from the film.

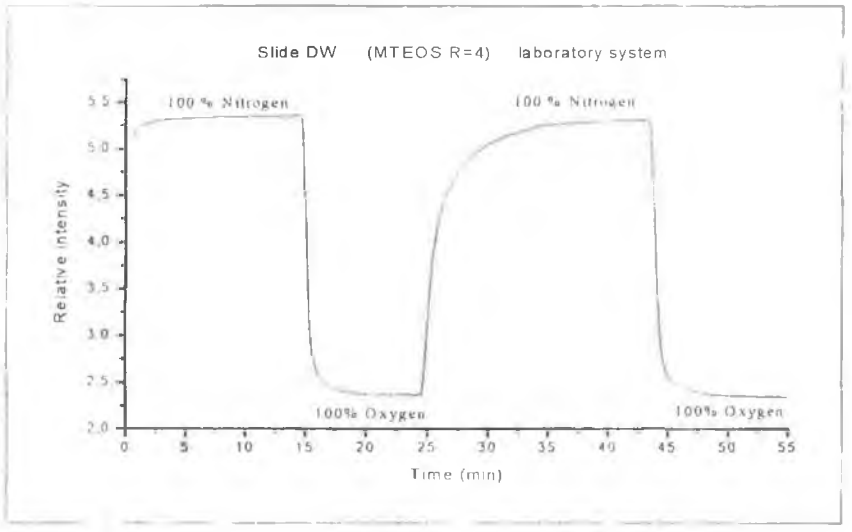

Figure 5.6: Typical sensor response obtained with the laboratory system.

The sealed cell is nearly three times bigger in the prototype than in the laboratory system. Because of this large volume, and because a metallic O-ring was needed to fix the slide on the sensor head and seal it, the equilibrium in the sealed chamber was obtained after a long period of time. To make the measurements quicker, each time the Oxygen/Nitrogen ratio was changed with the mass flow controller, the cell was emptied of water by flowing air instead of water, and was then filled up again with a gas saturated water with the new ratio. This technique might have influenced the results as the film was in contact with air (which means a level of 20 % of Oxygen) between each measurement.

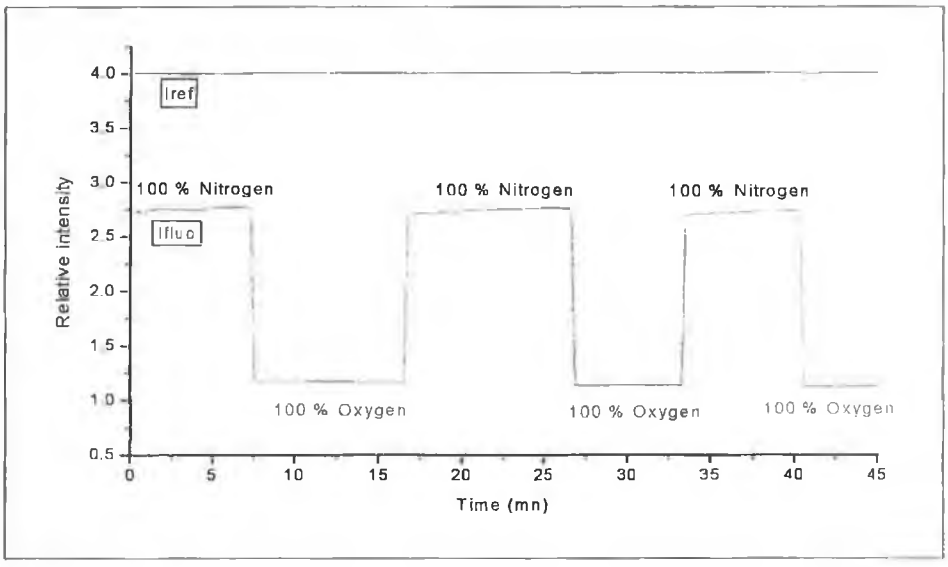

Figure 5.7: Typical graph obtained with the prototype.

Therefore, the curves obtained with the prototype (Cf. Figure 5.7) looked like square signals as the response time associated with the fill time of the cell was removed. By flowing air in the cell between each measurement, the oxygen molecules were more easily removed from the film and the new ratio of gas saturated water could take effect sooner.

Sealed chambers with smaller volumes would have given faster results. Such volumes as 9 cm^3 or 25 cm^3 are far bigger (10^5 times bigger) comparing to some other sensors which have a cell volume of 80 µl [1].

5.5. Film thickness measurements

5.5.1 Introduction

Some fundamental film characterisation and optimisation studies were done as part of this work. This included film thickness measurements and measuring quenching as a function of thickness (Cf. Chapter 6).

A UV-VIS spectrophotometer (Cary WinUV, Varian Australia Pty Ltd) has been used to measure the thickness of the sol-gel films. This method is based on the measurement of the transmission spectrum and therefore requires non-absorbing coating. A set of undoped films has been made up for this purpose.

The thickness measured is not the true thickness of the doped film as there is no ruthenium in the coated solution. According to the good reproducibility of dip-coating films, the difference in the thickness obtained for different undoped films should be the same as the difference obtained with doped films, as it is not the thickness itself that is interesting but the difference of thicknesses. The fact that the ruthenium is not added does not matter.

This method of determining thickness is usually limited to cases where films are thicker than 300 nm. Thickness measurements will be presented in Chapter 6.

5.5.2 Technique

The thickness can be determined from the transmission spectra from the position of the interference maxima [3]. The basic condition for interference fringes when light is passed through a thin film is:

$$2\,n\,d = m\,\lambda \qquad [5.1]$$

Where: d: thickness of the film,

n: refractive index of the film,

m: fringe number

λ: wavelength of light

The film thickness *d* is obtained from the following equation:

$$d = \frac{\Delta m}{2n_c\left[\frac{1}{\lambda_1} - \frac{1}{\lambda_2}\right]} \qquad [5.2]$$

with: n_c: refractive index of the coating (1.43 for the sol-gel films)

Δm: order of separation of the maxima.

λ_1 and λ_2: wavelength positions of the extrema.

This parameters can be seen in Figure 5.8.

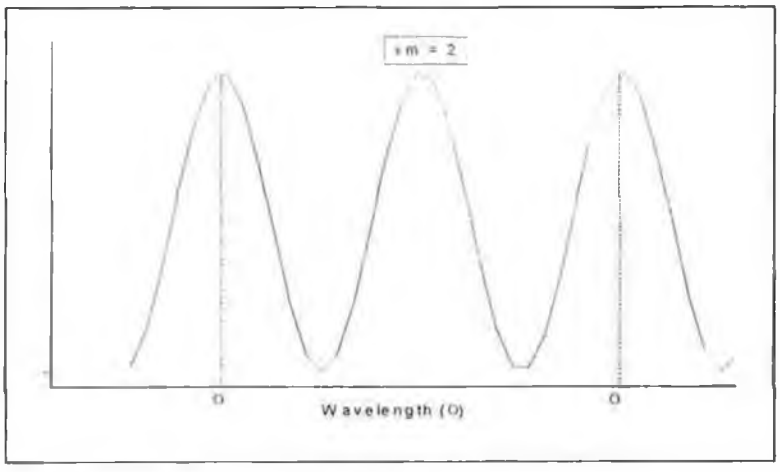

Figure 5.8: Interference fringes.

5.6 Conclusion

This chapter outlined the design of the prototype sensor and its developments from a laboratory-based configuration to a commercial instrument, which means a portable and miniaturised sensor, easy to use and low cost. All the different components of the sensor have been described in detail. A comparison between the use of the two instruments has also been discussed. Finally the technique used to measure the film thicknesses has been described.

The following chapters will discuss the measurements taken with the instruments over a period of time of 12 months.

References:

[1] Martin M.F. Choi, Dan Xiao, **"Oxygen-sensitive reverse-phase optode membrane using silica-adsorbed ruthenium(II) complex embedded in gelatin film."**, Analytica Chimica Acta 387, 197-205, 1999.

[2] A. Mills and Q. Chang, **" Modeled diffusion-controlled response and recovery behaviour of a naked optical film sensor with a hyperbolic-type response to analyte concentration"**, Analyst, 1992, Vol. 117, pp. 1461.

[3] O.S. Heavens, **"Optical properties of thin solid films"**, Dover Publications, New-York, 1965.

Chapter 6: Film characterisation

6.1 Introduction

This chapter presents some studies of film characterisation and optimisation which were carried out in parallel with the sensor development and testing. Section 6.2 contains some discussion and results on dye leaching. Section 6.3 presents some data on the influence of film thickness on quenching and Section 6.4 looks at the silicone rubber optical isolation layer.

6.2 Leaching studies

It has been observed that some sol-gel coatings tend to release some of the incorporated dye when immersed in aqueous solution [1,2]. This dye leaching is due to the fact that the dye complex is not chemically bound but merely physically entrapped in the sol-gel matrix. This causes a reduction in fluorescence intensity, which is clearly undesirable for optimum sensor performance.

Previous leaching studies carried out in this laboratory [3] using a technique where the film fluorescence was monitored over a period of days in flowing water, indicated that the degree of leaching varied with R value (water to precursor ratio, Cf. Chapter 4). In these studies R=2 MTEOS films exhibited considerably more leaching than R=4 films. As a result of this, R=4 MTEOS films were chosen as the optimum films for sensor applications.

As part of this project, it was decided to use a different approach to the study of leaching effects. Instead of monitoring the film fluorescence, the film was immersed in stirred water or flowing water in a closed system for various periods of time and the resulting fluorescence of the water was then checked for evidence of dye fluorescence.

The study was done with water for two different film formulations. No evidence of leaching in water was found for the MTEOS R=4 films normally used for the sensor (here referred to as H-films). This is consistent with the previous work using the alternative approach.

Some leaching was detected for R=2 H-films, again consistent with previous work. This is shown in Figure 6.1. Here the 600nm peak is due to the ruthenium dye fluorescence. The other peaks including the large 530 nm peak are due to water Raman [4] which unfortunately could not be referenced out due to a fault in the software of the spectrophotometer.

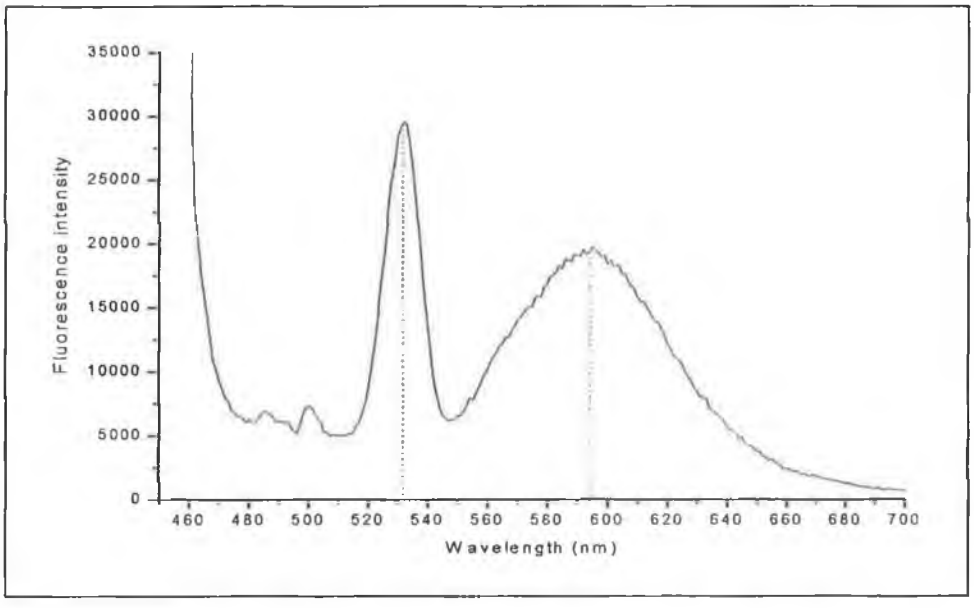

Figure 6.1: Leaching test (MTEOS R=2 slide), after flowing water for 90 min.

Note that the R=4 films have a denser microstructure resulting in smaller pores compared to R=2. This accounts for the reduced leaching effect. During the project an alternative film fabrication procedure (resulting in films referred to as films C) was investigated as this sol was more viscous giving rise to thicker films (see next section). The procedure is shown and compared to procedure H in Table 6.1.

In gram	Procedure C	Procedure H
Ruthenium dpp	0.025	0.0162
Ethanol	3.0	4.1508
Water pH=1	1.6	1.0376
MTEOS	4.0	2.568

Table 6.1: Ruthenium Sol-Gel procedures for MTEOS R=4.

When leaching studies were performed on these films, again no leaching was obtained. This study agrees with previous work and indicates that R=4 MTEOS films (both H films and C films) exhibit minimal leaching so the dye is sufficiently entrapped in the sol-gel matrix.

6.3 Film thickness measurements

During the course of this project the sensor films used were R=4 MTEOS-H-films (as discussed above) which were dipped at a fixed speed (0.99 mm/sec) giving a thickness of ≈ 250 nm. It had been observed in other oxygen-related work in the laboratory, that the quenching coefficient seemed to increase to a high value for very thick films, i.e. films coated using other techniques, for example stamping.
It was decided to do a controlled study on this effect to see if the quenching increased in a predictable way as thickness increased. The main motivation for the study was the need for thicker films (giving higher intensity) for another related project.

As in Section 6.2, the two different R=4 MTEOS films were used. The initial approach was to perform multiple dips, thus building up the film thickness. The thickness was monitored using the spectral transmission technique described in Chapter 5. For this, undoped films had to be fabricated as the dye fluorescence interfered with the thickness measurement as discussed. Thus, the thicknesses measured were not the real thicknesses of doped films, but gave a true indication of the relative thicknesses of the films. Figure 6.2 is shown as an example of the film thickness data. Note that with this technique, the film thickness measurement error is 30 nm.

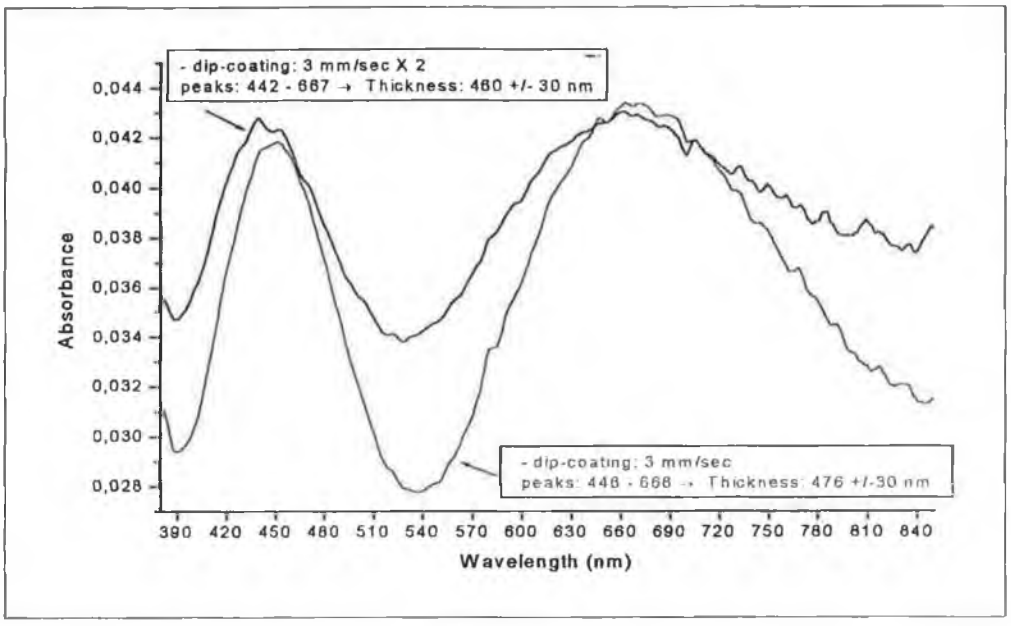

Figure 6.2: Film thickness measurements for normal and double dip-coated slides at 3mm/sec speed.

Table 6.2 shows the thickness results for film H for single, double and triple dipping at 0.99 mm/s and also for some higher speeds. It is clear that the thickness is not increasing as one would predict. The expected result would be that the film dipped three times at 0.99 mm/s should have thickness three times thicker than 250 nm. During this dipping procedure, the time between dips was varied (from a couple of minutes, or after one hour or one night in an oven at 70 °C) but to no avail. Note that the sol for H films is very non-viscous so it is concluded that this formulation is not suitable for this multiple dip procedure.

Dip-coating speed	Dip-coating layers	Thicknesses (in nm +/- 30 nm)
0.99 mm/sec	1	240
0.99 mm/sec	2	258
0.99 mm/sec	3	257
2.5 mm/sec	1	467
3 mm/sec	1	475
3 mm/sec	2	460

Table 6.2: Thicknesses vs dip-coating speed.

Table 6.3 shows that the quenching for the H films does not show any discernable increase for film thicknesses from 250 nm to 450 nm. Three different dip-coating speeds were used: a normal speed (0.99 mm/sec, the usual speed used all along this project), a low speed (0.20 mm/sec) and a fast speed (3.00 mm/sec). The last column of this table shows the results for a blobbed film (i.e. a droplet of sol allowed to dry) where a larger value of 74% is observed. This larger quenching for the much thicker film (thickness not easily measurable as an even surface is required for the thickness measurement technique) is likely due to the different drying process present due to increased thickness. Clearly the average pore size is larger in the thicker film, hence the higher quenching.

Slide	**1**	**2**	**3**	**4**	**5**	**6**
dip-coating speed in mm/sec	Normal 0.99	Normal 0.99	Normal 0.99	Low 0.20	fast 3.00	blob
coated layers	1	2	3	1	1	1
Quenching (in %)	**60.1**	**61.0**	**60.5**	**60.5**	**60.0**	**74.5**

Table 6.3: Quenching/intensity vs thickness.

The data obtained for C-films were better than above. The increased viscosity of this formulation appears to facilitate the multiple dip procedure, so the thickness does indeed build up although not exactly in multiples. The thickness data is shown in Table 6.4. Here the maximum thickness is higher than 2 μm. The error is quite large in the dipping procedure. For example, for double coated slides thicknesses were found to be between 1.3 and 2.3 μm.

According to the thickness measurement technique explained in Chapter 5, the more peaks obtained the thicker the film is. For example, as shown in Figure 6.3, twelve peaks were obtained for this double coated slide (speed coating: 3 mm/sec), which gave a thickness of 2330 nm or 2.3 μm.

Coating Characteristics	Dip-coating characteristics	Thickness (in nm +/- 30 nm)	Peaks number
single coated slides		825	5
		875	5
Double coated slides	After 1h	1390	7
	After 1h	1440	7
	After 1 night	1635	9
	After 1 night	2330	12
Triple coated slides	After 1h After 1 night	2325	12
	After 1h After 1 night		
	After a few minutes	1164	6
Quadruple coated slide	After a few minutes	2347	12
Quintuple coated slide	After a few minutes	1489	8

Table 6.4: Thickness vs dip-coating using films made with procedure C.

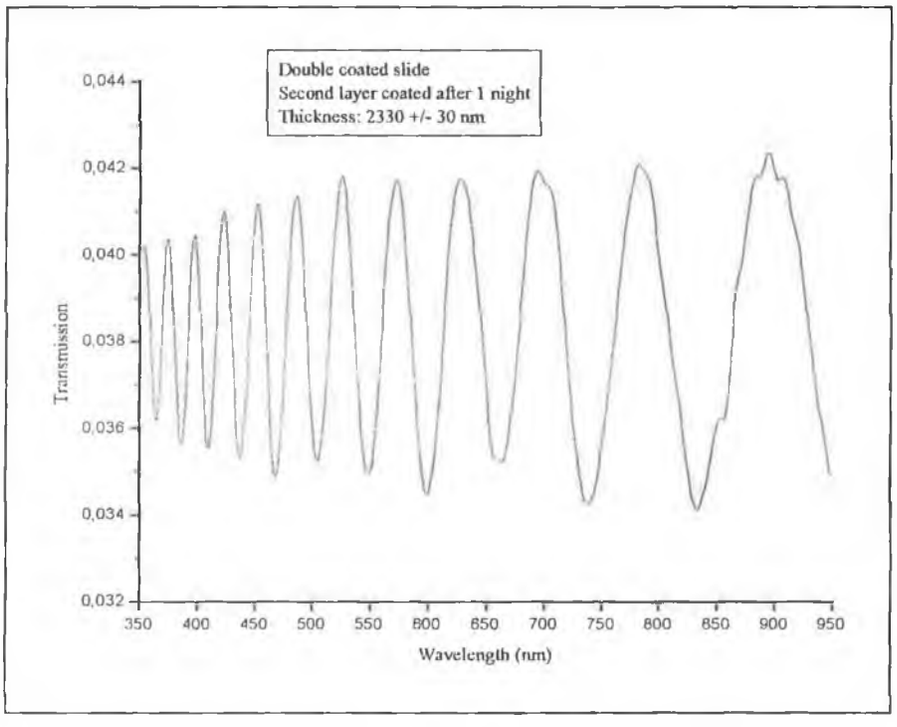

Figure 6.3: Transmission spectrum for a double coated slide, C-film.

Table 6.5 shows the corresponding quenching and intensity data. The intensity increases as expected with thickness. The second column specified the ambient temperature under which the measurements were held. It was found that under a warm ambient temperature (≈ 25°C) the fluorescence intensity obtained for 100 % nitrogen was increased by 0.5V (i.e. 4.7 % the value), and by 0.3V (i.e. 3.6 % of the value) for 100 % oxygen. This may be due to a shift in the LED spectrum (Cf. Chapter 7), giving rise to fluorescence intensities. Nevertheless the quenching values obtained under a warm temperature were lower than those obtained under normal ambient temperature (≈ 18°C).

Slide	Day temperature*	Coated layers	Dip-coating characteristics	Fluorescence intensity (100% N_2)	Quenching
1	normal	1		3.08	60.4 %
2	normal			3.20	59.7 %
3	**hot**	2	**After 3 hours in the oven**	**4.61**	**65.7 %**
4	normal		After 3 hours in the oven	3.83	66.7 %
5	normal		After 1 night in the oven	5.07	64.9 %
6	**hot**		**After 1 night in the oven**	**4.86**	**65.4 %**
7	**hot**	3	**After 3 hours in the oven, and 1 night in the oven**	**7.35**	**66.4 %**
8	normal		After 3 hours in the oven, and 1 night in the oven	6.60	67.9 %
	hot			**6.44**	**67.1 %**

*hot: ≈ 25°C, normal: ≈18°C.

Table 6.5: Quenching vs thickness using films made with procedure C.

Figure 6.4 shows the fluorescence intensity (with 100 % N_2 saturated water) dependence on film thickness. Figure 6.5 shows the quenching as a function of thickness. The maximum quenching for a 2 μm film is ≈ 68 %, comparing to ≈ 60 % for a 250 nm film, so the effect is small. This indicates that the "blobbed" film in Table 6.3 must be extremely thick, as it shows a quenching value of 74.5 %.

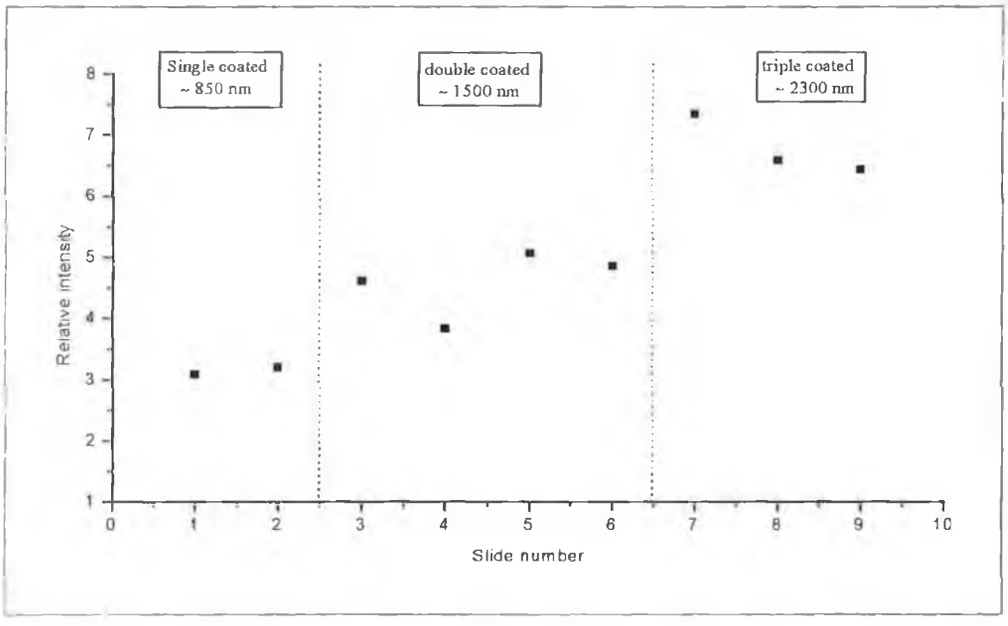

Figure 6.4: Relative intensity vs film thickness.

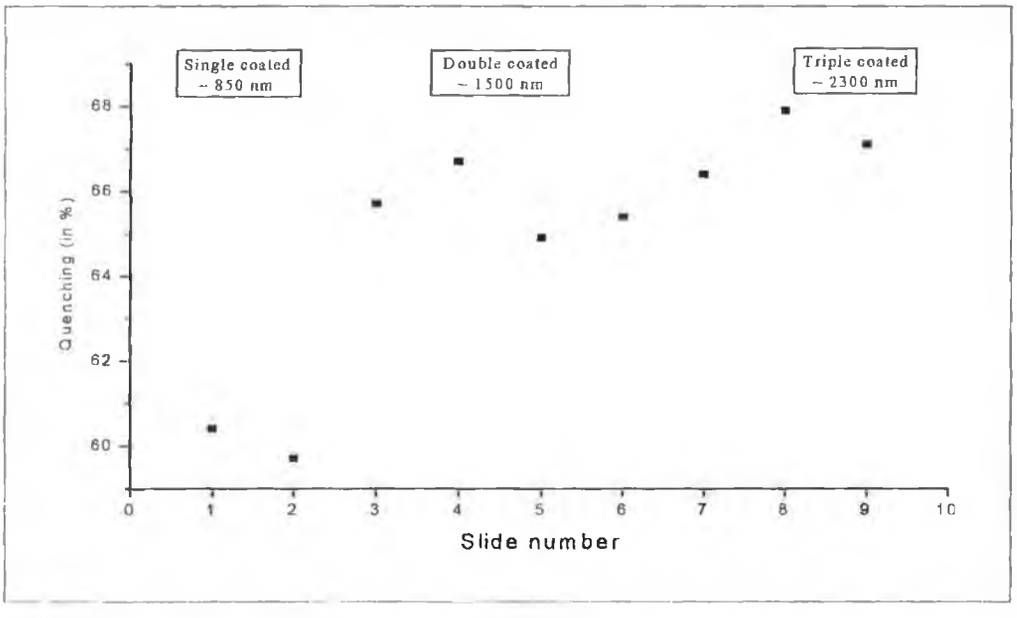

Figure 6.5: Quenching vs thickness.

In conclusion the increased quenching effect as a function of thickness has been demonstrated, but only for the C-films, due to the higher sol viscosity. It is proposed that this effect is a result of the different drying profile in the microstructure as a function of thickness. This is affecting the average pore size and ultimately the oxygen diffusion coefficient and the quenching. It is an interesting effect and requires further investigations. It may have implications for the sensor development as thickness reproducibility will need to be established in order to produce films with reproducible quenching values.

6.4. Black silicone rubber

Previous studies have been done to optimise the black silicone rubber [5,6], an optical isolation layer which reduces interferences from ambient light or background fluorescence, on the oxygen sensitive film measurements. Moreover, this black silicone layer makes the signal independent of the optical properties of the surroundings (e.g. refractive index, turbidity reflectivity, or coloration), and acts as a barrier to potentially interfering ionic fluorescence quenchers, such as heavy metals. Also the silicone rubber is hydrophobic, which is a great advantage concerning biofouling. Some results are presented here, which investigate the effect of the rubber layer on quenching and also characterises the transmission properties.

This silicone rubber was made using 62 % toluene as solvent [5]. In a cuvette, 3.8mg of Wacker N189, black rubber silicone, were added to 62mg of toluene. After mixing strongly, the cuvette was put in a beaker and left in an ultra sound wave bath for 30 minutes in order to get a homogeneous mixture.
The silicone rubber was then dip-coated at a 0.99 mm/sec speed over the ruthenium film. The film was dried at ambient temperature, and not used for a few days.

A first test was run in air, with a blank slide dip-coated with black silicone rubber. The intensity results obtained with or without the flow cell on did not show much difference (Cf. Figure 6.6), which means that the black rubber silicone layer was working as an optical isolator. There was only 0.19V difference in the relative voltage, which corresponds to less than 0.2 % although the intensity obtained with a

blank slide without the flow cell on could not be recorded as the signal was saturated (at 12V). The 0.19V difference compared to the signal obtained with a blank slide was less than 0.02 % of maximum voltage (12V).

It is concluded that the black rubber silicone was thick enough to avoid interferences from ambient light.

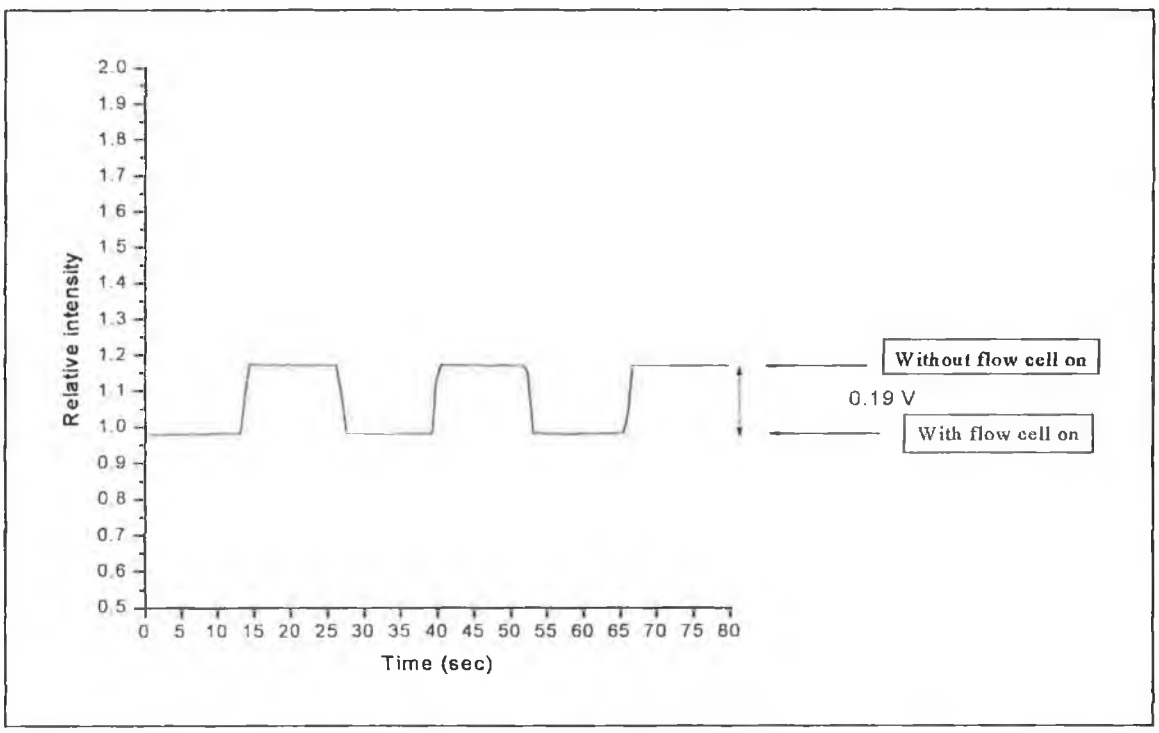

Figure 6. 6 : Black rubber silicon coated on a blank slide, with and without the flow cell.

In order to check any effect on quenching, the quenching has been recorded before and after adding the black silicone layer over the sol-gel ruthenium film.

This study was done on the laboratory system. The results obtained for both tests, with and without the silicone rubber layer, were similar (Cf. Table 6.8). The first measurement taken after dip coating the black silicone rubber seemed to give much higher quenching. This could be due either to an instability of the laboratory system, or to any effect due to the first measurement. If this data is cancelled, then the measurements altogether give a standard deviation of only 0.78, which is 1 % of the value.

The black rubber silicone layer dip coated over the thin film did not affect the quenching result of the film, and the different measurements showed a good stability of the coating.

	Without silicone rubber		With silicone rubber			
Time	first test	3 weeks later	first test	1 week later	1 month later	9 months later
Quenching (%)	66.77	66.74	71.42	67.93	66.56	66.85

Table 6.8: Quenching before and after coating the black silicon rubber on the same slide.

Another test has been done on the prototype system within 3 days. Both of the slides chosen had been dip-coated with the same sol-gel solution on the same day, and should therefore have the same behaviour. According to Table 6.9, no difference appeared in the Stern-Volmer coefficient comparing the slide coated or not coated with black rubber silicone.

	Slide with silicone rubber		Slide without silicone rubber
Date	first test	1 day later	2 days later
Stern-Volmer coefficient	0.0170	0.0159	0.0170

Table 6.9: Stern-Volmer coefficient with or without the black silicon rubber coated slides.

6.5 Conclusion

It appears that the sol-gel protocol which gave the best results were the "MTEOS R=4, procedure H" and that the best substrate was the glass slide. No dye leaching appeared with these films, which means that there was no reduction of the fluorescence intensity. Nevertheless, it appeared that to obtain thicker films with the dip-coating method, procedure C was more suitable because of the higher viscosity. The increased quenching effect as a function of film thickness was confirmed and needs further investigations.

Finally, the black rubber study showed that coating a black rubber silicon layer on a sol-gel-coated glass slide does not affect its behaviour. Hence, the quenching, as well as the Stern-Volmer coefficient remained the same before or after the coating.

References

[1] S.C Kraus, R. Czolk, J. Reichert, H. J. Ache, **"Optimisation of the sol-gel process for the development of optochemical sensors"**, Sensors and Actuators B, 1993, Vol. 15-16, pp.199-202.

[2] Butler T.M., MacCraith B.D., McDonagh C., **"Leaching in Sol-gel-Derived Silica Films for Optical pH Sensing"**, Journal of Non-Crystalline Solids, 1998, Vol. 224, pp. 249-258.

[3] A. Shields, **"Development of an Optical Dissolved Oxygen Sensor"**, MSc. Thesis, Optical Sensor Group, Dublin City University, 1999.

[4] J. R. Lakowicz, **"Principles of Fluorescence Spectroscopy"**, Plenum Press, New-York and London, 1986.

[5] M. Niggemann, Optical Sensor Group, Dublin City University, unpublished results, 1998.

[6] The American Society of Limnology and Oceanography, Inc., **"Fiber-optic oxygen microsensors, a new tool in aquatic biology"**, Limnol. Oceanogr., 40(7), 1995, 1159-1175.

Chapter 7: The prototype

7.1 Introduction

This chapter presents measurements carried out with the prototype sensor. It highlights in particular the importance of the baseline and temperature effects in the reproducibility of the measurements. The stability of the LED and insertion reproducibility of the slide is investigated. Finally measurements in marine water are presented.

7.2 Reproducibility of the measurements

Figure 7.1 shows a typical calibration response obtained with the prototype sensor. This response was obtained by flowing water containing different oxygen concentrations through the flow cell. Note that the quenching was calculated from equation 3.12 taking two baseline readings before and after the measurements, which help to correct for the drift (mentioned later). Temperature was also monitored. The signal was stable, but each single measurement did not give the same result each time while using the same slide. Figure 7.2 shows the Stern-Volmer plot (Equation 3.10) calculated from calibrations carried out for one month with the slide DW (stored in deionised water). It highlights the instability of the Stern-Volmer coefficient over time. Table 7.1 emphasises these instabilities, as the quenching values (Q) and K_{SV} coefficients were changing and also gave different values depending on baseline value. The baseline signal was varying over 29 % of $Ib_{average}$. This means that if the quenching Q was calculated with the baseline value taken before or after the measurement, on average the results varied by 4.7 % of the $Q_{average}$. For the Stern-Volmer constant Ksv, on average the results varied by 27 % of the $Ksv_{average}$.

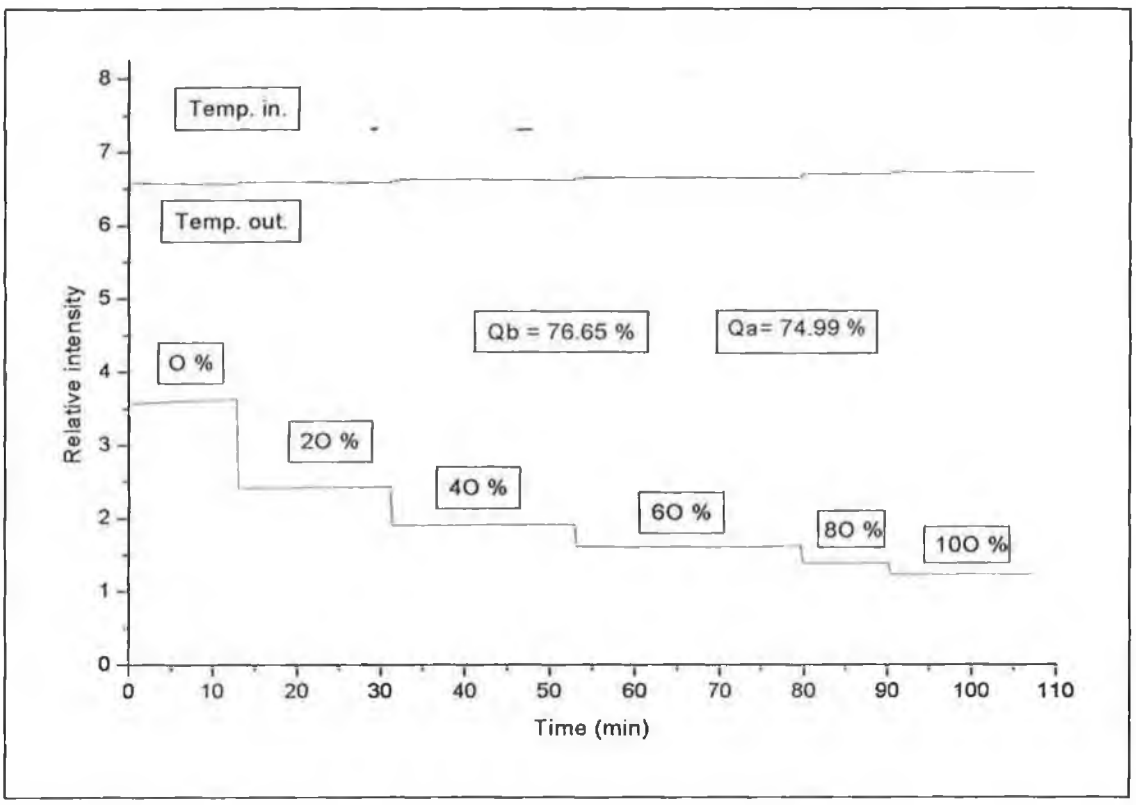

Figure 7.1: Calibration vs oxygen, quenching calculated before and after.

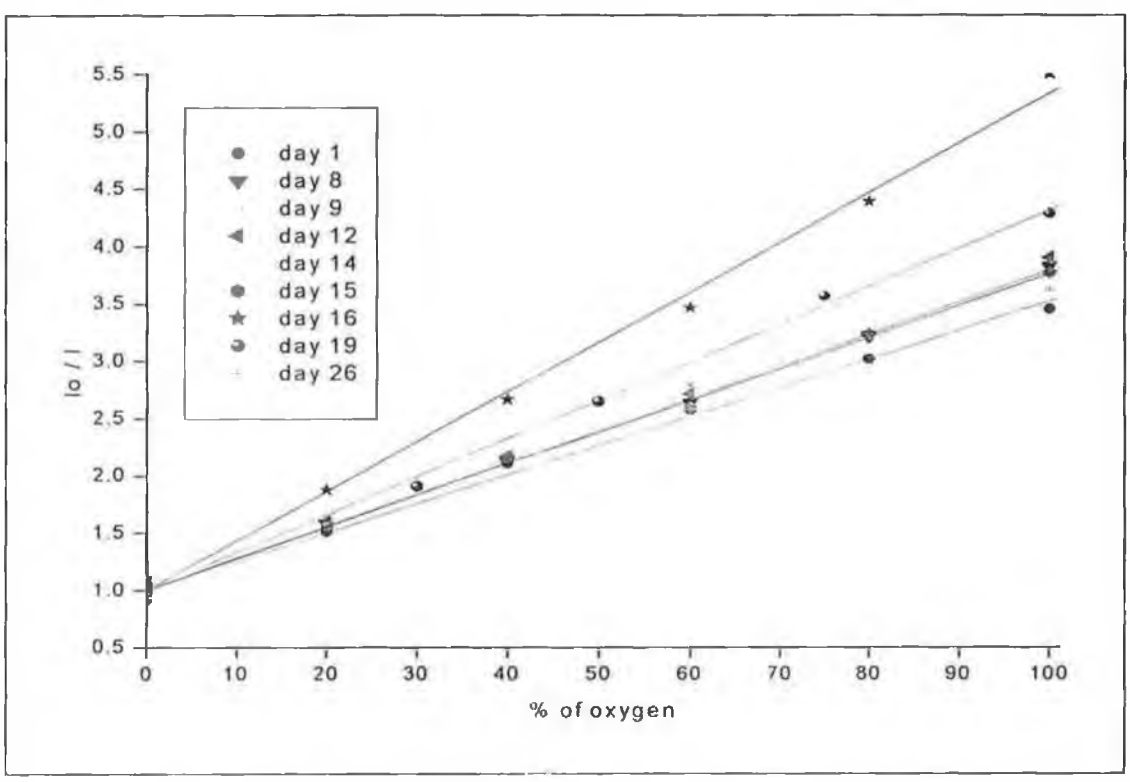

Figure 7.2: Stern-Volmer plots carried out within a month.

Day		1	8	9	12	14	15	17	19	27
100% N_2	I_{fluo}	4.25	3.72	3.52	4.27	3.71	3.51	3.57	3.70	3.74
	$I_{fluo} - I_{b\ bef.}$	3.57	3.11	3.00	3.12	3.32	2.93	3.24	3.14	2.94
100% O_2	I_{fluo}	1.57	1.23	1.17	1.72	1.19	1.13	1.05	1.30	1.47
	$I_{fluo} - I_{b\ after}$	0.97	0.84	0.80	0.85	0.87	0.84	0.83	0.74	0.81
$I_{b\ before}$		0.78	0.51	0.52	1.14	0.39	0.58	0.32	0.47	0.80
$I_{b\ after}$		0.70	0.39	0.37	0.87	0.33	0.29	0.22	0.57	0.77
ΔI_b		0.08	0.12	0.17	0.27	0.07	0.29	0.10	0.10	0.14
%		**12.5%**	**27.7%**	**37.4%**	**27.9%**	**17.7%**	**77.7%**	**37%**	**19.7%**	**19.2%**
$I_{o\ before}$			3.27	3.28	3.7	3.33	3.47	3.34	3.17	2.85
$I_{o\ after}$		3.35	3.21	3.18	3.31	3.35	3.17	3.47	3.19	2.93
$Ksv_{before}\ 10^{-4}$			343	400	492	315	508	350	283	337
$Ksv_{after}\ 10^{-4}$		252	279	297	287	349	278	433	331	277
$\Delta K_{sv}\ 10^{-4}$			74	103	207	34	230	83	48	70
%			**20.7%**	**29.7%**	**32.4%**	**10.2%**	**58.5%**	**21.2%**	**15.7%**	**19.7%**
Quenching $_{before}$		75.49	77.85	78.77	81.41	75.90	81.22	77.47	73.25	77.21
Quenching $_{after}$		73.42	73.99	74.78	74.92	74.57	73.91	75.15	75.55	73.70
ΔQ		2.07	2.87	3.98	7.49	1.34	7.31	2.32	2.3	3.51
%		**2.8%**	**3.8%**	**5.2%**	**8.3%**	**1.8%**	**9.4%**	**3.0%**	**3.1%**	**4.7%**

Table 7.1: Calibration obtained within a month, with a slide stored in deionised water.

It was thought that the reasons for these differences in quenching values and Stern-Volmer constants were mainly due either to the temperature variations of the baseline intensity (Cf. Section 7.3) or to the insertion variability (Cf. Section 7.7), or to both of these effects.

7.3 Variations of the baseline

The baseline intensity gave the background for the measurement. As explained previously, it was given by the photodiode recording the fluorescence while measuring the signal with a blank slide, i.e. without any fluorescence coming from the dye. As the acquisition program could not record negative values, it was necessary to offset the level of the baseline to a positive value (0.4V for example) in order to check any drift. Before giving any result this intensity had to be subtracted from the fluorescence intensity signal, to give the fluorescence from the dye only.

As shown on Figure 7.3, the baseline intensity fluctuated in inverse ratio with temperature. This baseline instability due to temperature fluctuations introduced an error into the quenching data, as the baseline intensity was part of the calculation (Cf. Equation 3.12).
According to Figures 7.4 a and 7.4 b, a linear (inverse) dependence of Ib vs temperature was found. It was thought that by plotting Ib vs temperature a reproducible temperature coefficient could be calculated but this was complicated by two effects:

(i) Some fluctuations in the temperature generated non-linear effects in the plot of Ib vs temperature (Cf. Figures 7.5). Those fluctuations were mainly due to the environment of the room (air-conditioning system cooling down the room and variations of the ambient temperature) but also sometimes to a warming up of the water flowing in the system, and may be the system by itself.
The extremum reached by the temperature after 3 hours (Cf. Figure 7.5 a) gave a discontinuity in the graph of Ib vs temperature (Cf. Figure 7.5 b), though the slope did not change. Each slope is a linear fit of points monitored in two time intervals, i.e. from 6.12 p.m. to 8.10 p.m. for the first one and from 8.13 p.m. to 7.45 a.m. for the second one. The second linear fit shows a shifted slope comparing to the first one. Although this shift or discontinuity looks like a hysteresis effect, there is no explanation about it. This discontinuity shows the extreme difficulty of this method to be used as a correction factor.

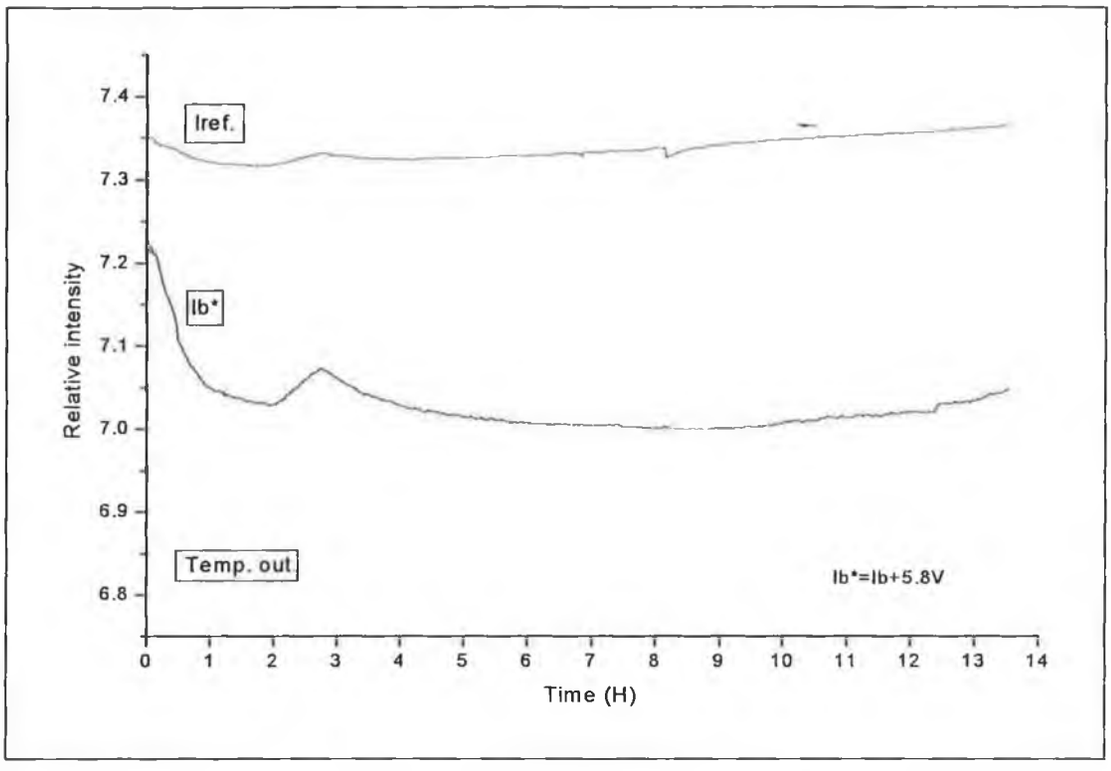

Figure 7.3: Baseline over a night (Ib* = Ib + 5.8V).

	Temperature Fluctuations	Δ (Ifluo./Iref.)	Slope Ifluo. vs t°	Slope Ifluo/Iref vs t°
Night (14 H)	Δ t° = 0.131 V		- 0.073	
Night (13 H)	Δ t° = 0.222 V	0.025	- 0.135	- 0.021
Night (13 H)	Δ t° = 0.222 V	0.022	- 0.113	- 0.020
Baseline (57 min)	Δ t° = 0.087 V	0.055	- 0.142	- 0.011
Night (13 H)	Δ t° = 0.584 V	0.055	- 0.128	- 0.021
Weekend (57 H)	Δ t° = 0.577 V	0.027	- 0.047	- 0.004
Baseline (55 min)	Δ t° = 0.254 V	0.024	- 0.078	- 0.018

Table 7.2: Slope coefficient vs Ib and temperature.

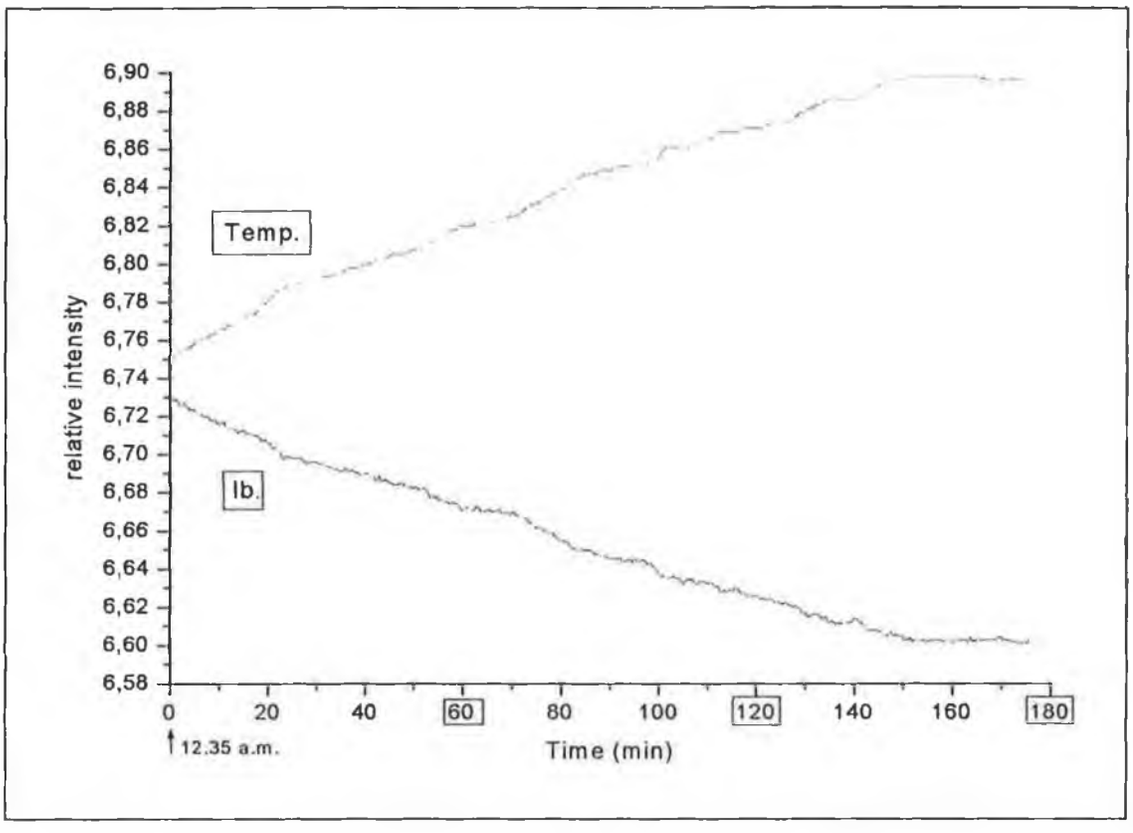

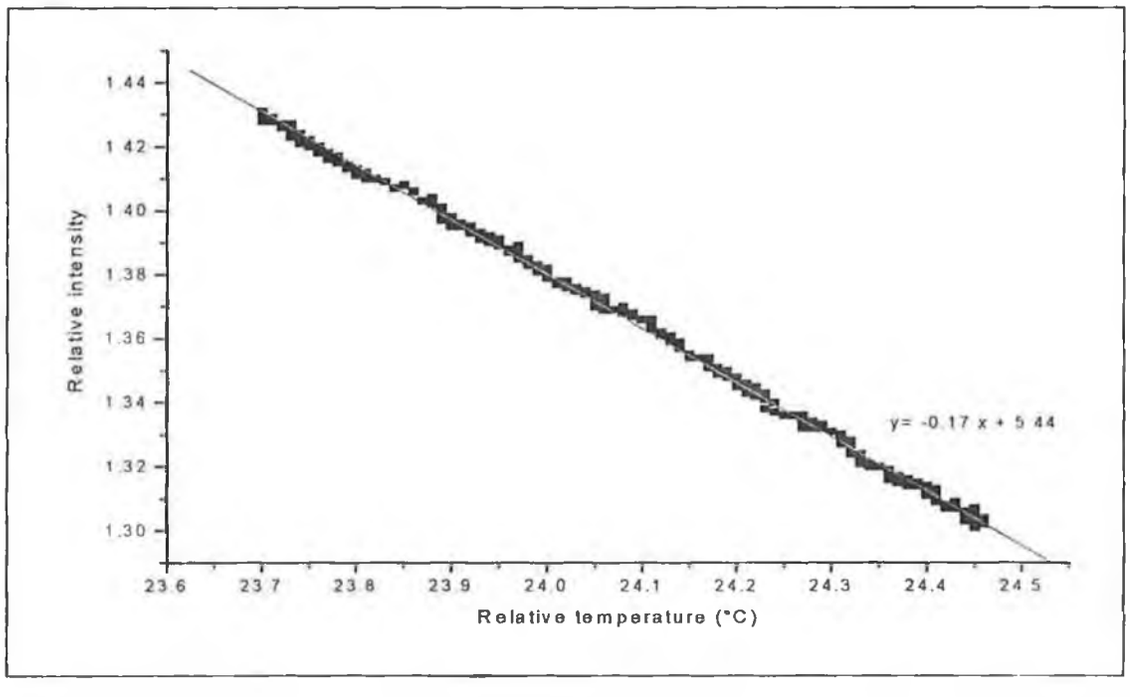

Figures 7.4 a and 7.4 b: Baseline plot and Ib vs Temperature plot.

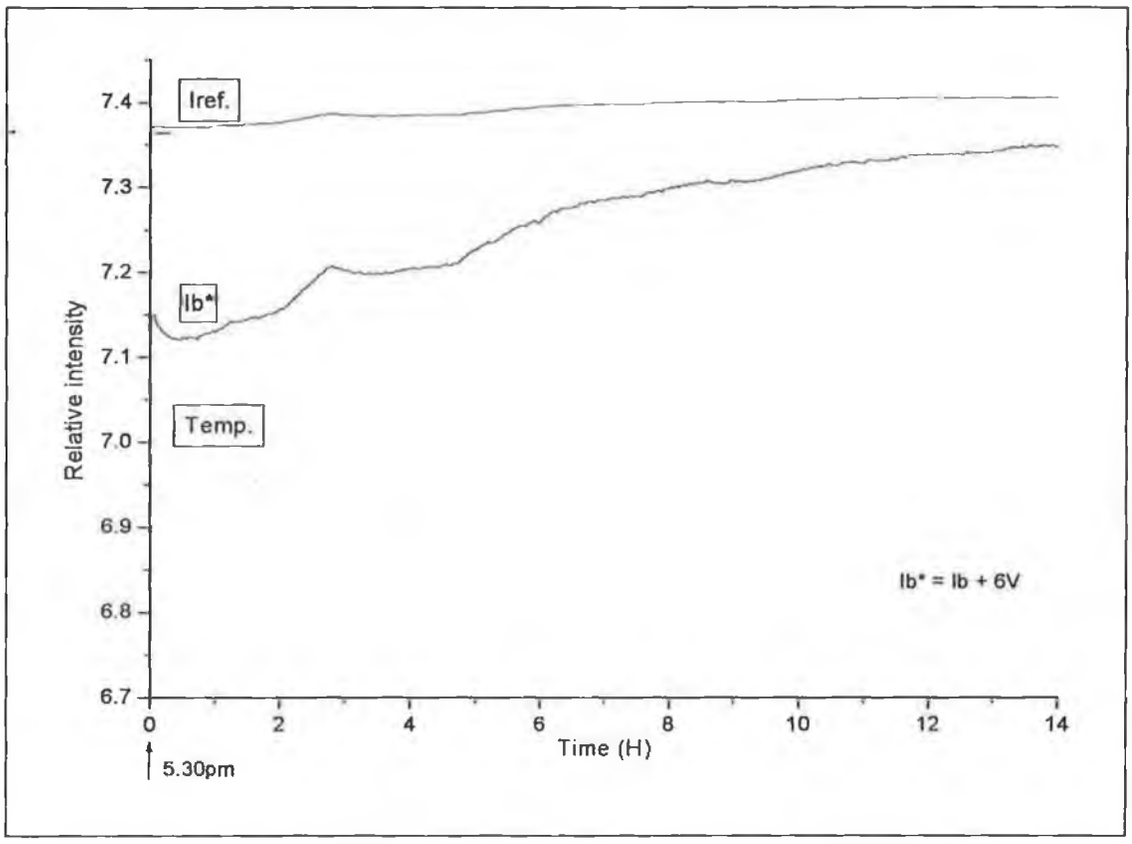

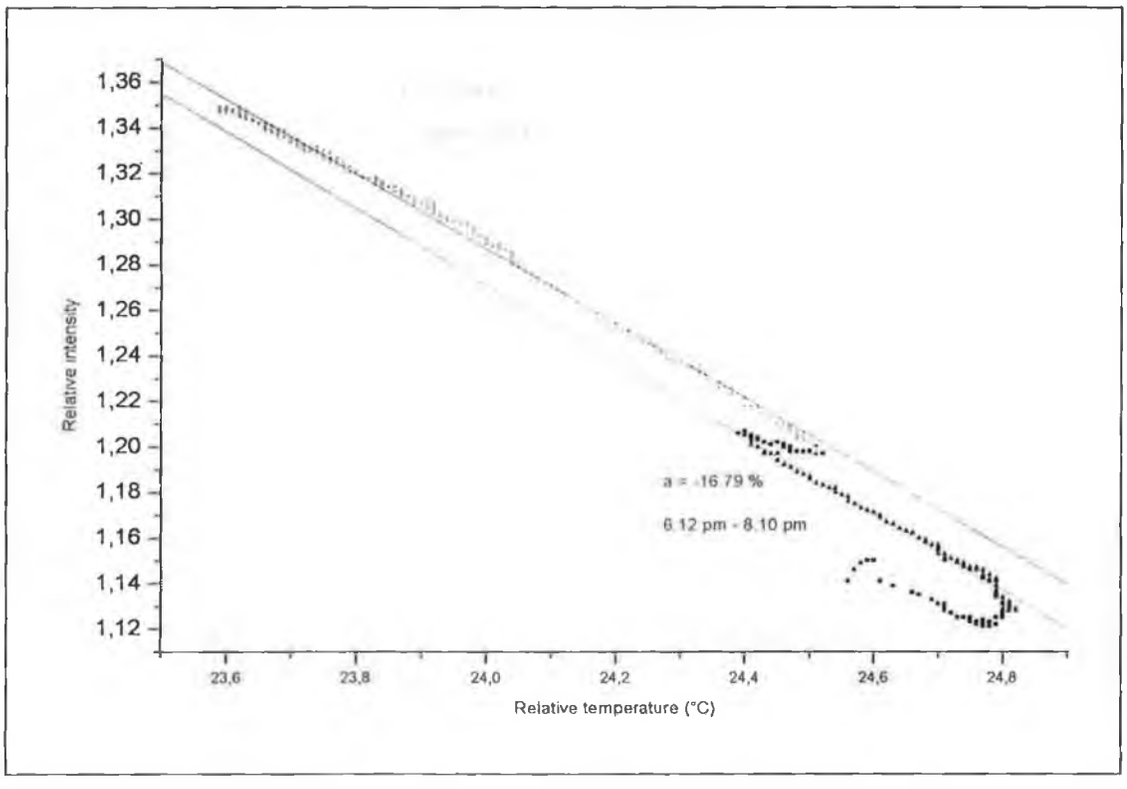

Figures 7.5 a and 7.5 b: Baseline plot and Ib vs temperature plot.

(ii) The measurement of different baselines did not give the same slope coefficient while plotting Ib vs temperature. Table 7.2 gives the different slope coefficients obtained for each baseline and the corresponding fluctuations (each arrow shows an increase or a decrease) in the temperature. Even for the same type of temperature fluctuations the slope coefficient was not the same. The first two measurements, for example, had the same temperature fluctuations, and were recorded for the same amount of time but gave a completely different result for the slope (- 0.073 and - 0.135).

Though the baseline signal depends directly on the temperature, it is not possible to find any reproducible correlation between both of those measurements as each single measurement gives a different result.

It was thought that any baseline fluctuations could be corrected by ratioing Ifluo/Iref (Cf. Figure 7.6). Unfortunately this proved not to be possible. Attempts were made to ensure that the Ifluo channel and Iref were matched in terms of amplification, both photodiodes being identical models. It was concluded (see next section) that the reference photodiode could not be used to correct for fluctuations.

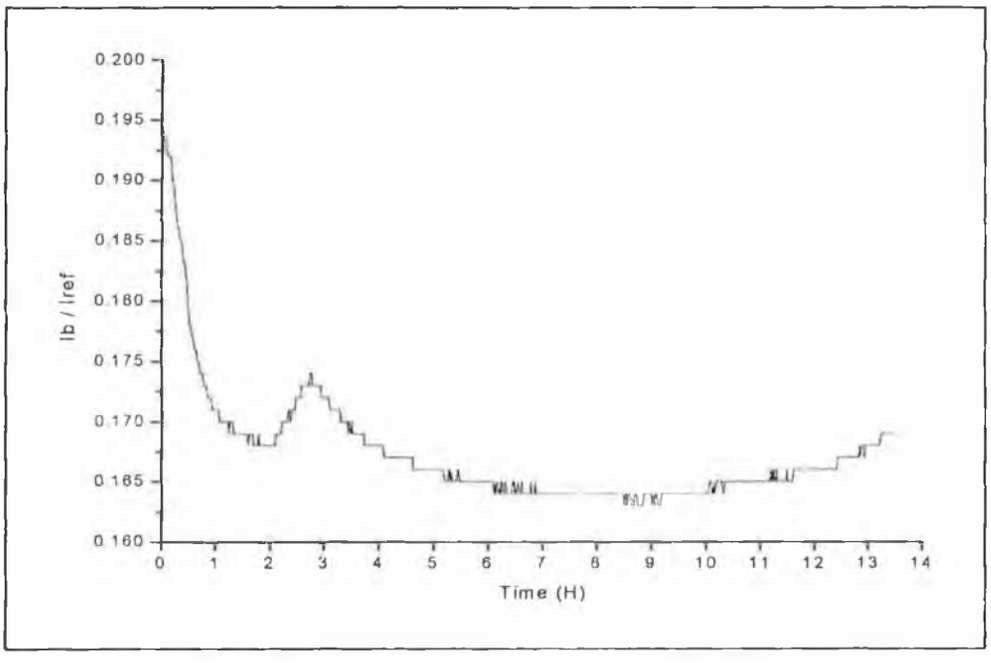

Figure 7.6: Blank slide, Ib / Iref ratio vs time.

7.4 Temperature dependence

As described in Chapter 5, the prototype was equipped with two temperature sensors, one recording the temperature of the water in the flow cell ("Temp. out"), and the other one recording the temperature inside the prototype close to the electronics and the LED ("Temp. in"). It was interesting to have two temperature sensors in order to evaluate the origin of the temperature fluctuations, which could be the prototype itself with a warming up of the electronics, or the ambient environment, or the flowing water.

According to Figure 7.7, the temperature recorded by both sensors seemed to follow the same curve. The temperature sensor outside just had some extrema higher than the internal temperature sensor.

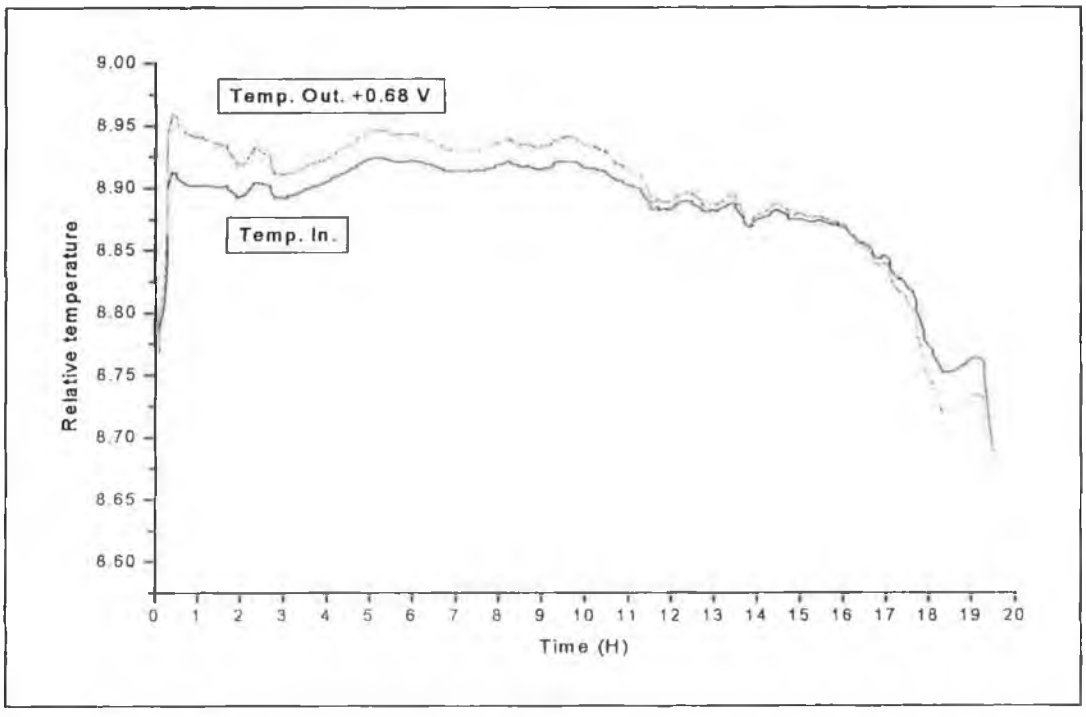

Figure 7.7: Temperature sensors inside and outside.

Figures 7.8 a and b, which plot the baseline intensity vs both of those temperatures, show that none of them gives a linear dependence

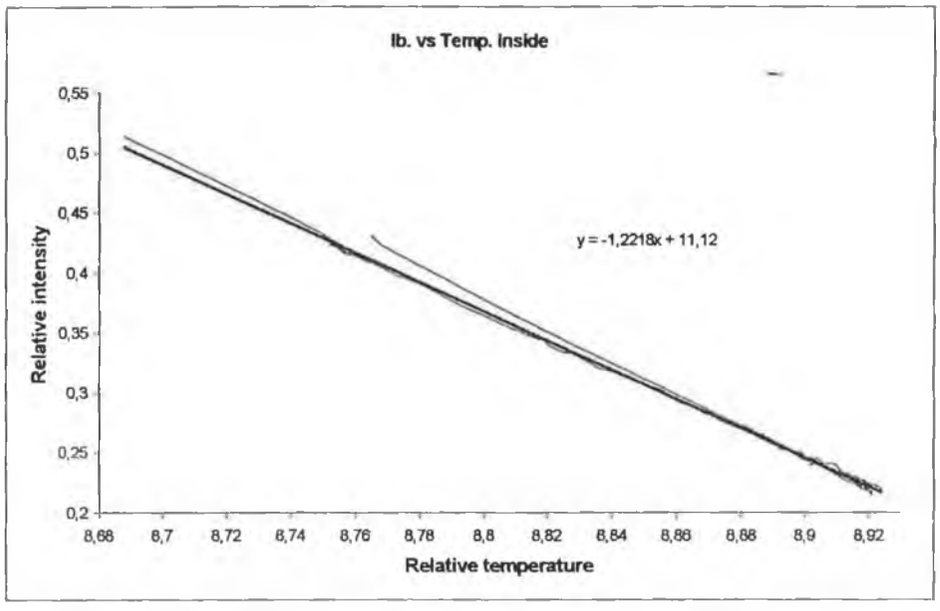

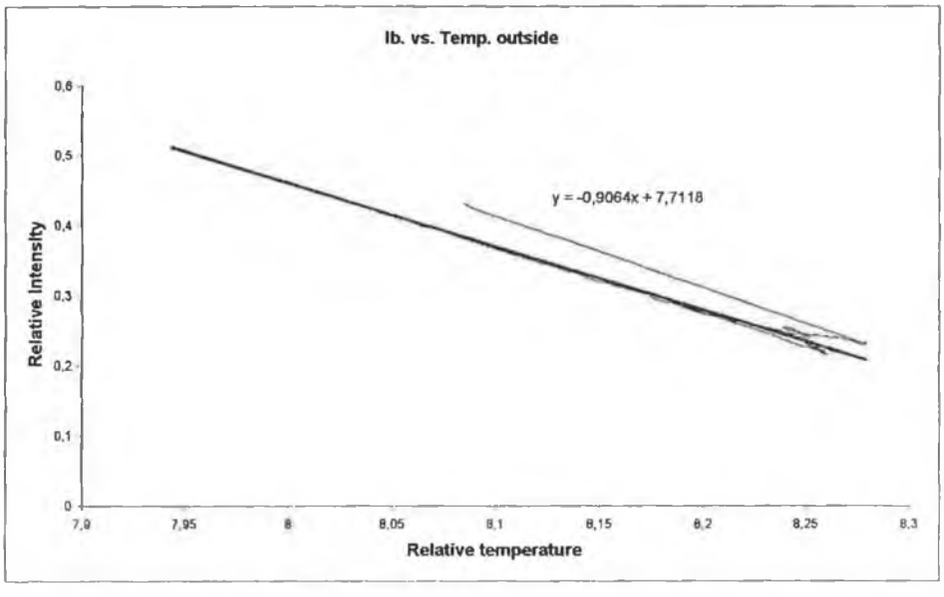

Figures 7.8 a and b: Ib vs temperature inside and outside.

According to Figure 7.9, both photodiodes monitoring the LED and fluorescence intensities did not have the same behaviour. Even if those two signals did not have the same amplification the second one seemed to be much more sensitive to the temperature. Though both of the photodiodes were identical, they did not have the same behaviour with respect to the temperature. Hence it was concluded that the reference photodiode cannot be used to correct for variations in the fluorescence photodiode.

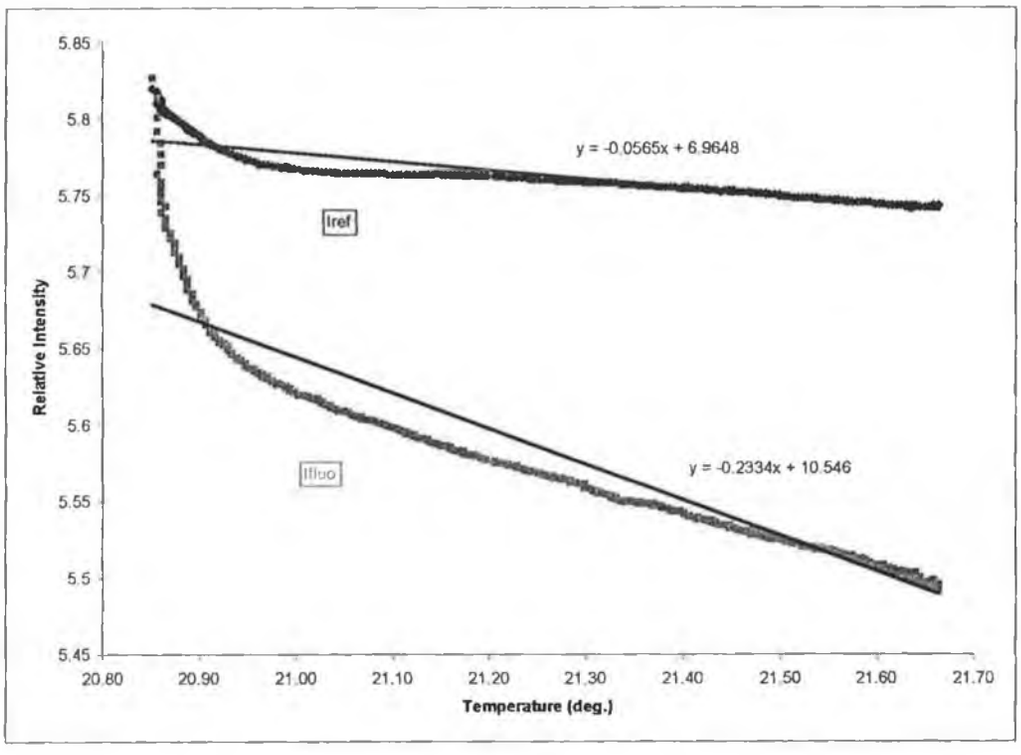

Figure 7.9: $I_{reference}$ and $I_{fluorescence}$ vs temperature.

Figures 7.10a and 7.10b show the variations in Ifluo and Iref signals and temperature signals respectively with the LED off. This was a crucial measurement. There was only 1mV of variation for 15 hours, for both of the signals (reference and fluorescence photodiodes) whereas the temperature was fluctuating between 0mV and 300 mV. The steps in Figure 7.10a were due to the acquisition card. The variations were so small that they reached the resolution limit of the analog to digital converter, which is 10 mV.

On the contrary, the results obtained with the LED on (Cf. Figure 7.7) gave a variation of 324 mV for the reference signal, and 228 mV for the fluorescence signal, while the temperature was fluctuating between 0 mV and 220 mV.

In conclusion there was no significant drift in the electronics. The drift or dependence in the reference and fluorescence signals must be mainly due to the fluctuations of the LED, which is discussed in Section 7.4.

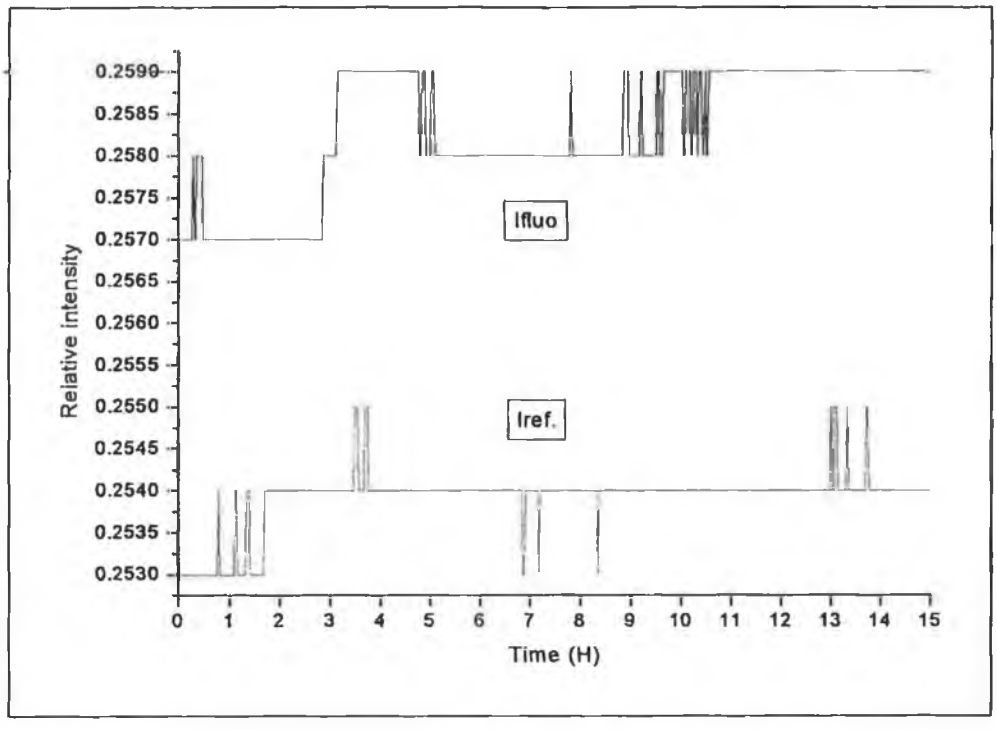

Figure 7.10a: Reference and fluorescence signals recorded with the LED off.

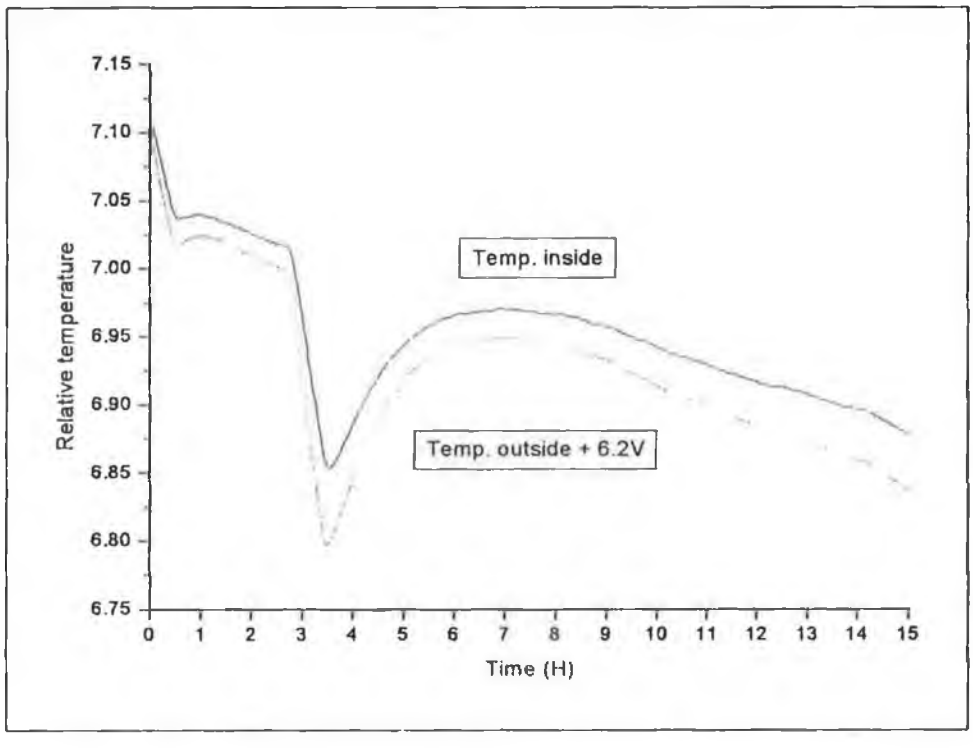

Figure 7.10b: Temperature signals recorded with the LED off.

7.5. LED

7.5.1 Instability of the LED

As seen in the last section, there was no significant drift in the electronics, so the variations in the baseline signal must be due to temperature effects in the LED.
The spectrum of the LED shows a peak at 474 nm. As the temperature increases the spectrum shifts slightly towards higher wavelengths (Nichia, Technical data) [1,2]. The spectrum also broadens out with temperature and the absolute intensity changes.
As the reference photodiode measures the wavelengths lower than 540 nm, it still records the maximum intensity of the light coming from the peak emission. Therefore, the reference photodiode does not see any difference with a small change in the temperature.
On the contrary, the fluorescence photodiode measures the light between 530 nm and 770 nm, which corresponds to the highest slope point of the peak. Therefore, with a blank slide (i.e. without fluorescence) the fluorescence photodiode records a variation of the intensity even with a slight change in the temperature.

7.5.2 Warming up time

As shown on the following graphs (Cf. Figures 7.11a and 7.11b), there was a warming up time of the LED. It took about an hour for the temperature inside the electronics to be stable. For about an hour the signal of the temperature sensor outside was increasing slowly (Cf. Figure 7.11a). This might be due to the influence of the warming up of the system (LED and electronics inside). By flowing water in the cell (Cf. Figure 7.11b), the stability of the temperature inside the system was obtained after only 25 min, while the temperature outside was relatively constant. This increase of temperature was mainly due to the system itself, and flowing water in the cell cooled down the system. To avoid this warming up time, the LED was left switched on all the time.

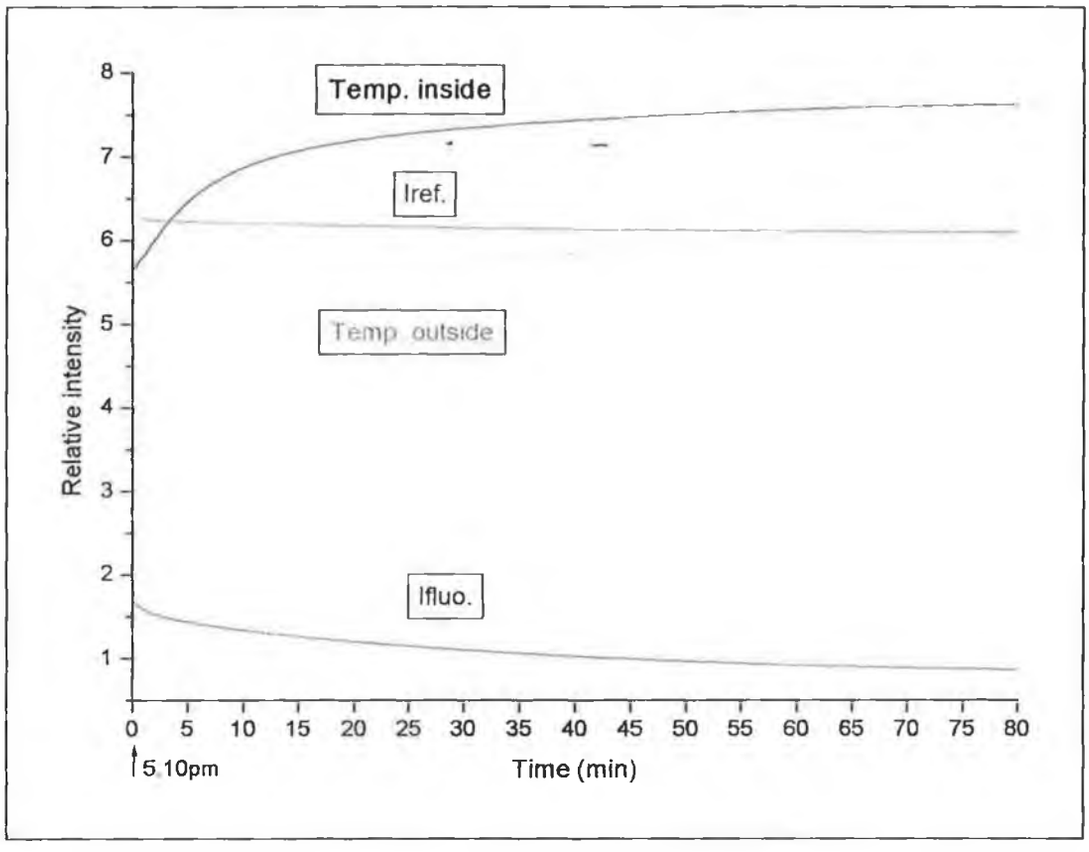

Figure 7.11a: Baseline and stability after switching on the LED (air).

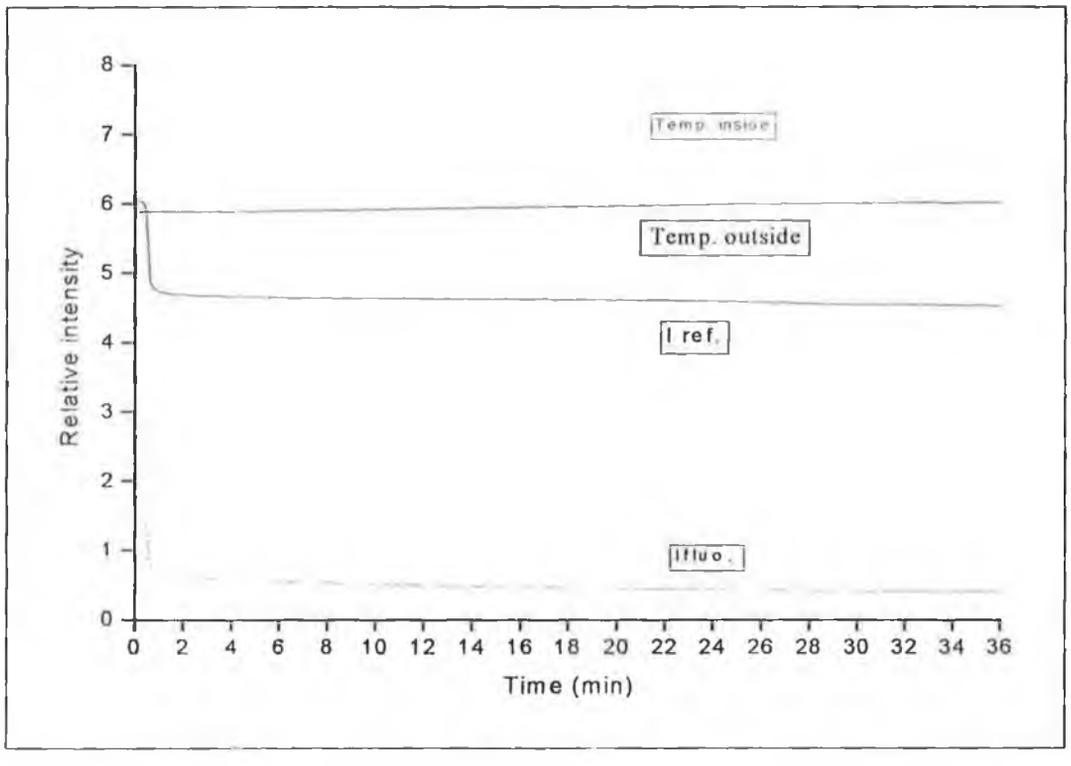

Figure 7.11b: Baseline and stability after switching on the LED (water).

7.6 Insertion problem

To check the reproducibility of the slide insertion in the sensor, the baseline has been recorded while removing a blank slide eight times during the measurement (Cf. Figure 7.12). Each single measurement gave a different result each time the blank side was removed.

It has to be noticed that for the fifth step, as the top of the sensor was not screwed enough at the beginning of the measurement, there was a significant increase of the intensity. But while the temperature was decreasing at the end, nothing was changing in the baseline signal.

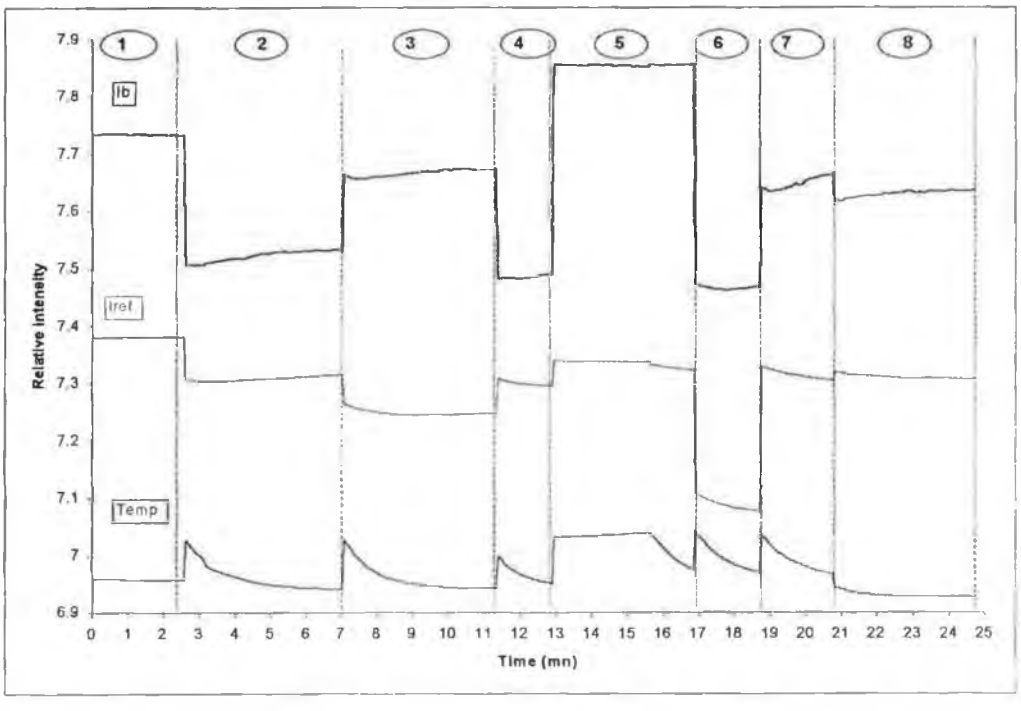

Figure 7.12: Baseline test, removing 8 times the blank side.

The two screws to fix the glass slide on the sensor's head resulted in a slightly different position (angle) of the slide. The results of a further test are shown in Figure 7.13. The screws were first completely tightened and measurements were taken as the screws were being unscrewed.

Figure 7.13 shows the different intensity in the baseline, as the screws were tightened to varying degrees. The shaded bars indicate the level of adjustment of each screw. At

the beginning, both of them were screwed at a maximum level, then the right one was unscrewed by a quarter turn, twice again, and then it was the turn of the left one. The seventh step, when both of the screws had been unscrewed by three-quarter turn, gave the same intensity as at the beginning. With the thirteenth step, the screws came back to their starting level, and so the intensity reached the same level as at the beginning as well.

The baseline intensity was extremely sensitive to this small difference in the angle of the slide, as just a quarter turn gave a difference of 0.17 V or 4.3 % of the value of the intensity.

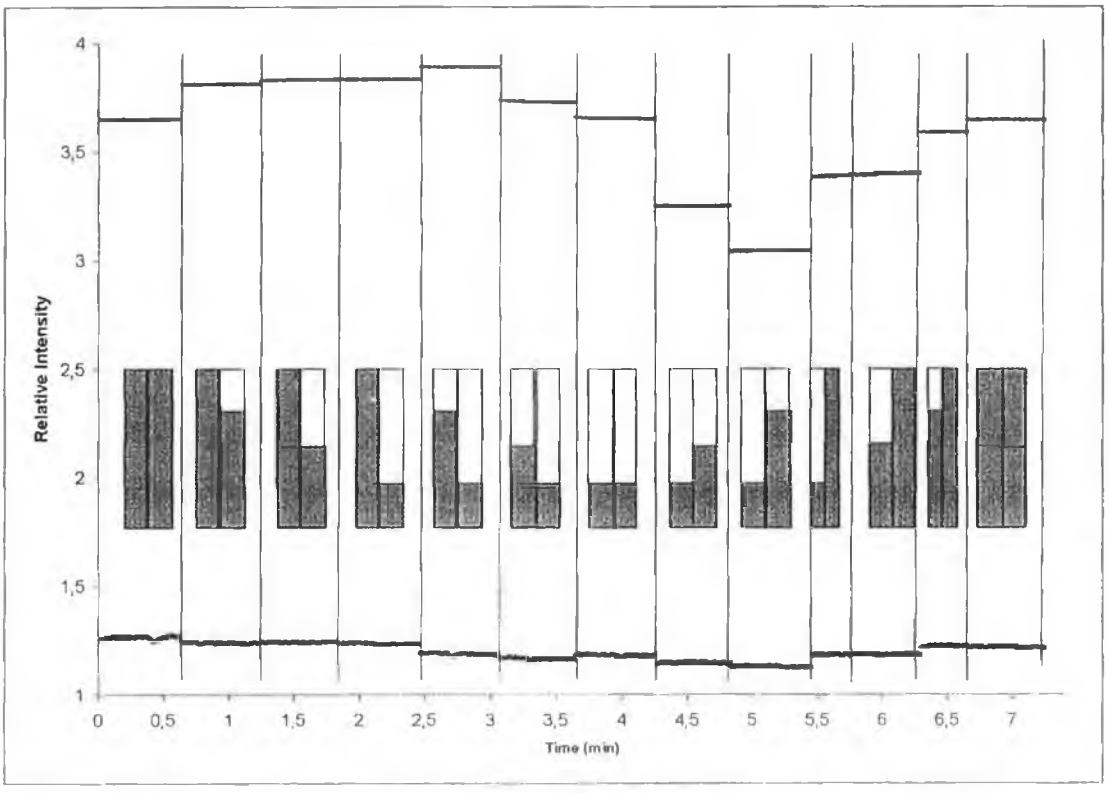

Figure 7.13: Insertion test.

It is clear that the problem highlighted above can best be overcome by fixing the slide in a more permanent way to the sensor head. However, for preliminary testing purposes this is difficult.

7.7. Marine water measurements

7.7.1 Introduction

According to M. L. Hitchman [3], the adjunction of salts in a gas saturated water does not affect the activity coefficient of the gas, provided that there are no chemical reactions between them. Nevertheless, the oxygen solubility is decreasing with increasing salt concentration. This behaviour is characteristic of the solubility of many nonelectrolytes when an electrolyte is added to the solution. It has been pointed out in Section 4.3 that the mechanism of oxygen sensing for this sensor is partitioning. The oxygen partial pressure is not affected and only the concentration of oxygen decreases with salinity. This phenomenon is known as the *salting-out effect* [4,5,6].
This study deals with any effect of the salts on the oxygen quenching. Note that measurements in this section were made with the prototype using an alternative LED which appears to have better temperature characteristics.

7.7.2 Seawater preparation

The artificial seawater samples have been made with a synthetic sea salt called *Instant Ocean®* and manufactured by Aquarium Systems (France). This salt, free of nitrate and phosphate, was used by other research groups for their laboratory tests. To prepare small quantities of seawater, 30g of *Instant Ocean®* salt was used for each litre of deionised water.

7.7.3 Measurements

The measurements were done at a constant salt concentration of 30 g/l, but at ambient temperature.
Different tests had been running for the saline water study (Cf. Table 7.3). For this purpose some tests had been done with deionised water and others in seawater. All of them were measuring the 0 % and 100 % oxygen levels (giving the quenching values

of the film). Only the last test was a calibration from 0 % to 100 % with increments of 5 % until 20 %, and 20 % until 100 % (Stern-Volmer plot).

Test	Slide characteristics	Water	Sensor
1	stored in seawater for 11 days	deionised water	Lab system
2	new	deionised water	Lab system
3	new	deionised water	Prototype
4	same as test 3	seawater	Prototype
5	same as tests 3,4	seawater	Prototype
6	same as tests 3,4,5	deionised water	Prototype
7	same as tests 3,4,5,7	deionised water	Prototype

Table 7.3: Deionised and seawater measurements with the lab system and the prototype.

To check any effect of the salt on the thin film two tests (test 1 and test 2) had been run in deionised water with the lab system.

The slide used for the first test was previously stored for 11 days in saline water, while the slide used for the second test was new (it had never been immersed). Comparing the results obtained with both slides would allow the detection of any effect of the salt on the film.

Prior to the test, both films were examined with a microscope and compared to a film stored for months in deionised water. It clearly appeared that all the surfaces were different. On the film stored in seawater, some salt crystals were deposited on it, which seemed quite normal as the film was dried at ambient temperature before the

examination. Nevertheless, the film previously stored in deionised water and then dried did not look the same as the film which had never been immersed. The data on these slides are shown in Figures 7.14 – 7.17.

The results obtained with both slides were relatively similar. The quenching values calculated with the baseline measured before and after the measurement were respectively 61.5 % and 60.5 % for the slide previously stored in seawater, and respectively 59.6 % and 59.0 % for the slide which had never been immersed.

It seemed that after being immersed for 11 days in seawater the film characteristics had not been damaged or modified. The quenching values obtained for both films were similar, the difference was only about 3 % of the value. Moreover, the time to reach the 100 % (or 0 %) oxygen level was identical in both cases.

To check any effect of the salt on the quenching measurement 4 tests (test 3 to test 7) were run in deionised water and seawater with the prototype.

The first test run in deionised water gave a quenching of 62 %.

The second test, run the following day, in seawater gave Q_b = 59.2% and Q_a = 58.4%.

The third test run in seawater the day after gave Q_b = 57.22 % and Q_a = 55.78 %.

The fourth test run in deionised water 10 days later gave Q_b = 59.3% and Q_a = 60.5%.

A Stern-Volmer calibration has been done in deionised water a week later, and gave quenching values of Q_b = 61.04 % and Q_a = 60.8 %.

The values of quenching obtained in seawater were relatively similar to those obtained in deionised water. The third test gave a lower quenching value, which could be due to a temperature effect as even the temperature inside the sensor (near the electronics) was unstable. The last two tests done in deionised water showed that the quenching values were still in the same range as the values obtained in deionised water before doing the tests in seawater.

The only difference in the results, which did not appear on the graphs, was that it took a much longer time to reach the first level of 100 % Nitrogen (or deoxygenated water) in seawater.

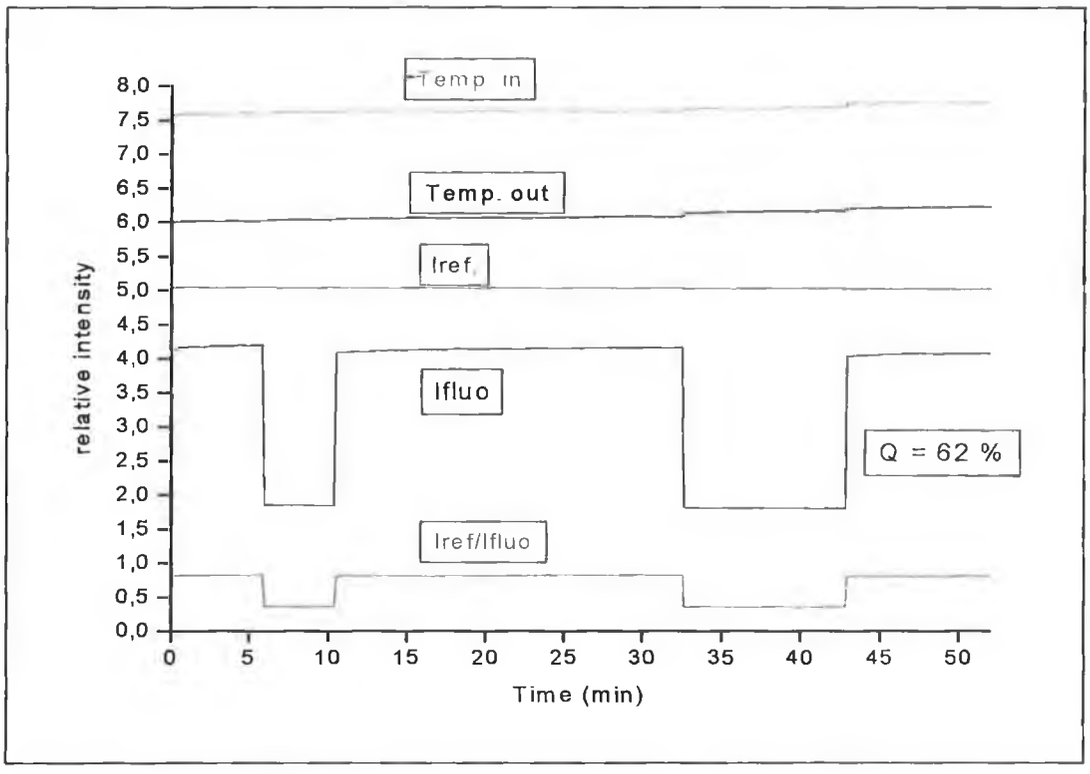

Figure 7.14: First test in deionised water, prototype.

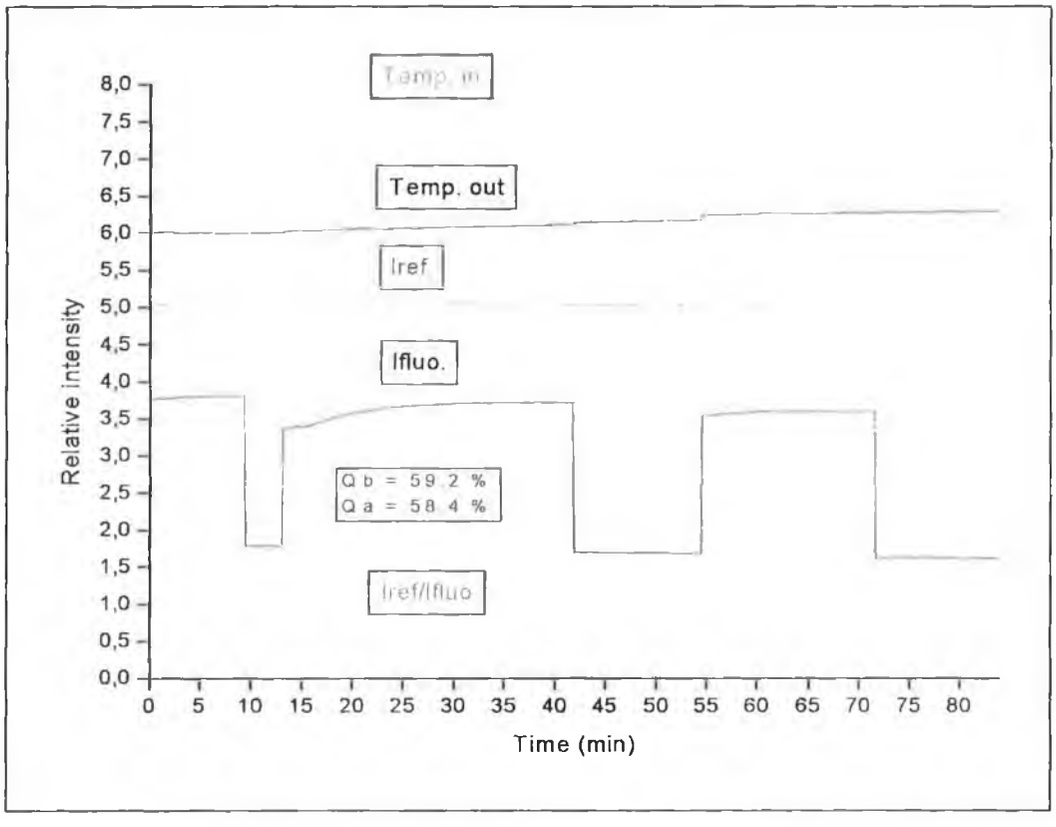

Figure 7.15: Second test in seawater, prototype.

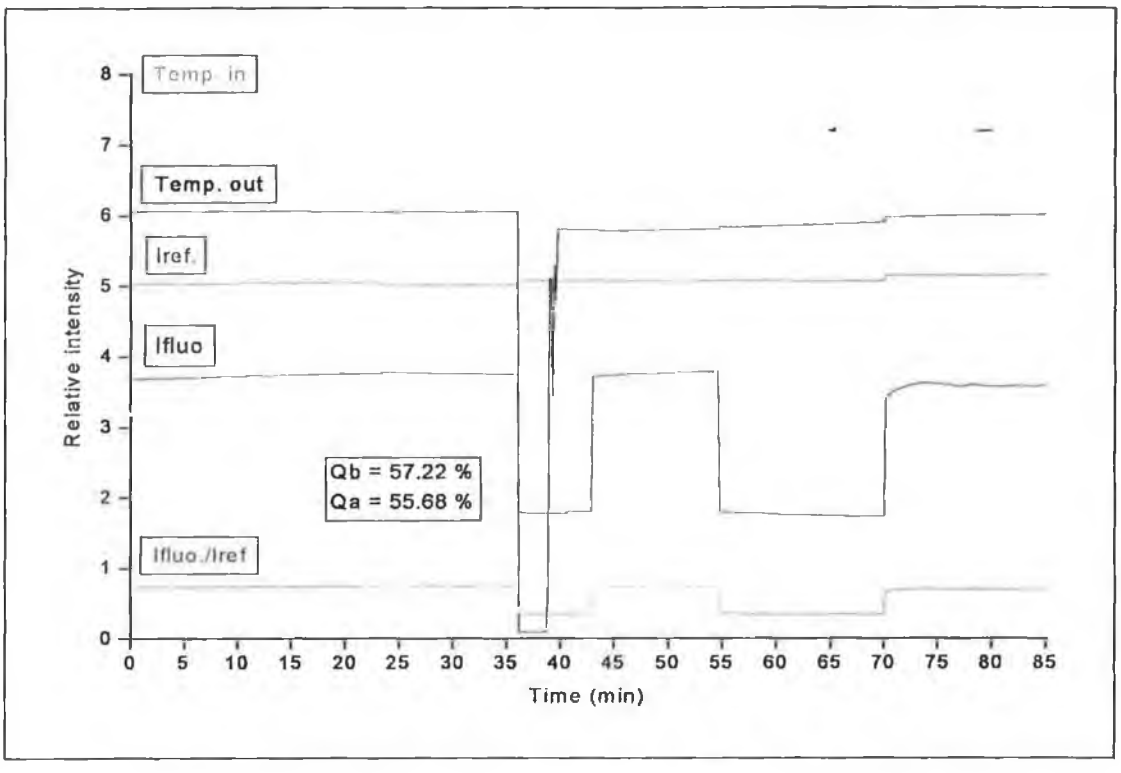

Figure 7.16: Third test in seawater, prototype.

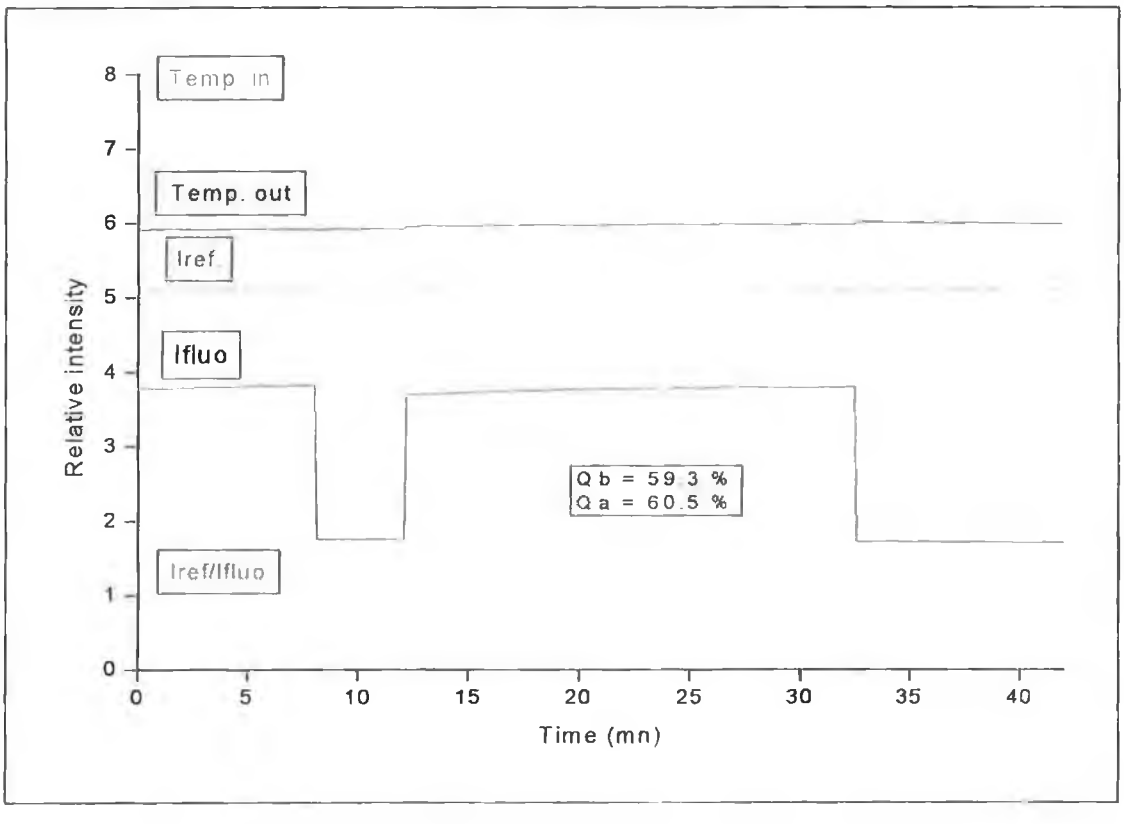

Figure 7.17: Fourth test in deionised water after 2 runs in seawater, prototype.

To confirm the results found with the quenching study in deionised water and seawater, three Stern-Volmer calibrations had been run with the same slide, in deionised water and seawater with the prototype, within two weeks (Cf. Table 7.4). The second test was run in deionised water. The results plot in Figure 7.18 show that the salt did not affect the Stern-Volmer coefficient K_{SV}.

Test	Time	Water	K_{SV}
1	first day	seawater	0.0159
2	12 days later	deionised water	0.0159
3	14 days later	seawater	0.0157

Table 7.4: Stern-Volmer coefficients in deionised and seawater measurements with the prototype.

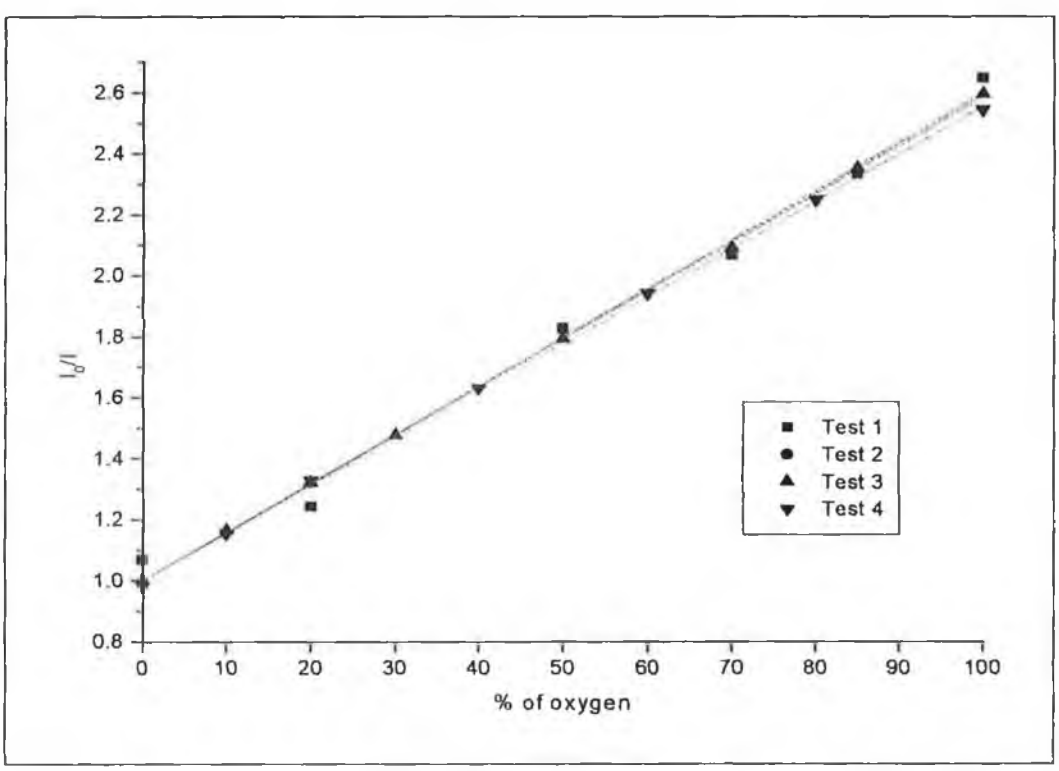

Figure 7.18: Stern-Volmer calibrations in deionised water and seawater, within two weeks with the prototype.

According to the different tests done in seawater and compared to deionised water tests, it appeared that the salt in water did not affect the quenching results given by the film. This result is in agreement with another study [7], where it was found that the salinity did not affect the quenching or the fluorescence lifetime.

7.8 Conclusion

This chapter highlighted in detail the measurements obtained with the prototype sensor, and emphasised the reproducibility problem due to the temperature dependence of the LED and mainly due to the difficulty of glass slide insertion reproducibility. A detailed comparison from measurements carried out in seawater and deionised water showed that the salts do not affect the quenching results.
The main issue for the use of the prototype will be to resolve the glass slide insertion dependence and the LED temperature effect.

References

[1] Tanaka Y., Toyamata T., tohmon R., **"A novel temperature-stable light-emitting diode"**, IEEE Transactions on electron devices, 41: (7) 1125-1127, Jul. 1994.

[2] Reynolds K.J., Dekock J.P., tarassenko L., Moyle J.T.B., **"Temperature-dependence of LED and its theoretical effect on pulse oximetry"**, British journal of Anaesthesia, 67: (5) 638-643, Nov. 1991.

[3] Michael L. Hitchman, **"Measurement of dissolved Oxygen"**, Ed. John Wiley & sons, New York, 1978.

[4] R. Battino and H.L. Clever, **"The solubility of gases in liquids"**, Chem. Revs., 77, 395, 1977.

[5] E. J. Green and D.E. Carrit, **"Oxygen solubility in sea water: thermodynamic influence of sea salt"**, Science, 157, 191, 1977.

[6] W.L. Masterson, **"Salting coefficients for gases in seawater from scaled-particle theory"**, J. Soln. Chem., 4, 523, 1975.

[7] J. F. Gouin, **"A fibre optic oxygen sensor for oceanography"**, IFREMER Brest, France, 1997.

Chapter 8: Measurements with the laboratory system and comparison with the prototype data

8.1 Introduction

As described in Chapter 5, a laboratory-based test system had been developed previously. Measurements made on this system are described and a comparison is made with the prototype measurements. Although the measurement protocol-technique was the same, there were important differences between laboratory-based and prototype systems. As the room where the laboratory system was set up was larger, there was a more constant temperature, so less variation in the ambient temperature. The smaller baseline drift in the laboratory system was also due partly to the fact that the electronics was in a separate unit from the sensor head. Finally the slide mounting technique was much more reproducible in the laboratory technique, minimising any insertion errors.

8.2 Comparison of quenching results

The slide used for the prototype measurements reported in Section 7.2 was also characterised using the laboratory system. This slide had been stored in deionised water for two months. Figure 8.1 shows the quenching (Q value) for this slide, measured over a period of time on both systems. The measurement period for the prototype was one month, while the same slide was monitored on the laboratory system over a period of three months. It was not possible to continue this particular study for more than one month on the prototype as a fault arose in the electronics which took some time to resolve.

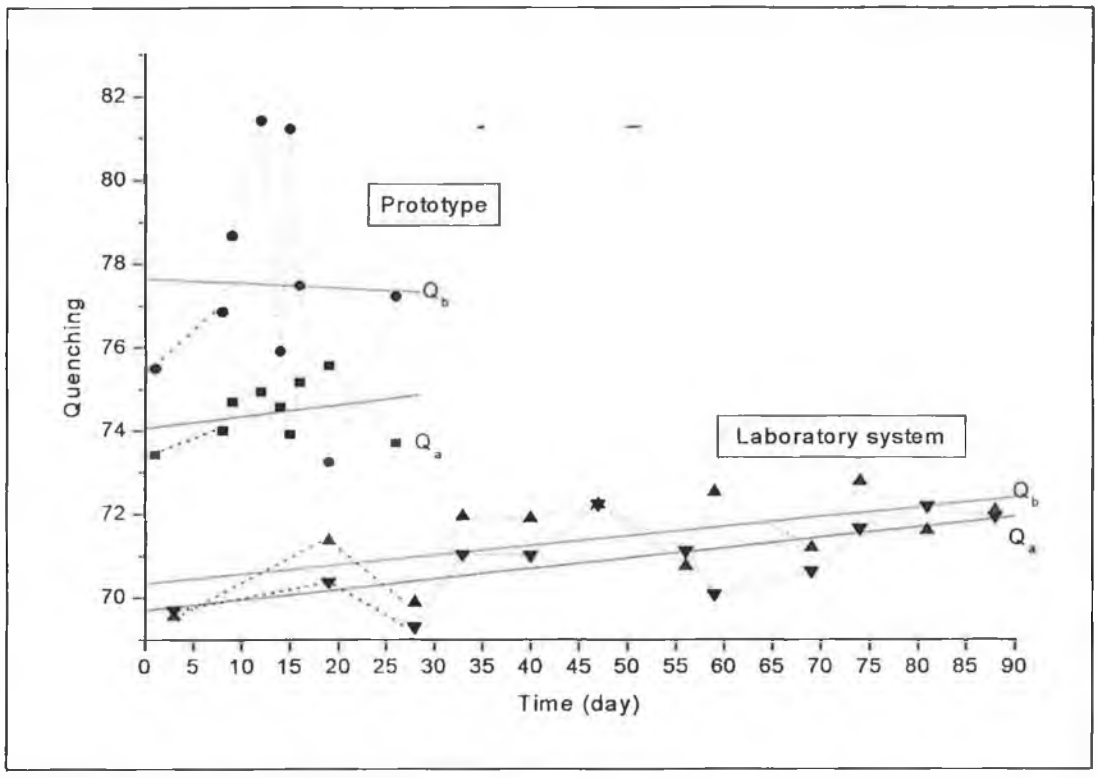

Figure 8.1: Fluctuations of the quenching over 1-3 months.

It is clear from Figure 8.1 that although the quenching values for the laboratory system show some variations with respect to baseline (i.e. the baseline measured before and after the measurement gives rise to an observable variation in Q) the variations are not as great as those obtained with the prototype system. These large fluctuations in Q-values for the prototype are consistent with the results reported in Section 7.2, and reflect the large temperature drift of the baseline. From the data (Cf. Appendix), the typical baseline fluctuations for the prototype were ranging from 10 - 40 %, while for the laboratory system the variations was ranging from 1 - 15 %, which implicated quenching fluctuations ranging from 2 - 9 % for the prototype and from 0 – 1 % for the laboratory system.

Figure 8.2 shows the same data expressed as K_{SV}, the Stern-Volmer coefficient. By comparing equations 3.6 and 3.11, it can be seen that the quenching value Q is related to K_{SV}. Any fluctuation in Q will manifest itself as a much larger fluctuation in K_{SV}. Hence, the K_{SV} variations for the prototype in Figure 8.2 were ranging from 10 – 30 %, while for the laboratory system they were ranging form 0 – 12 %. This indicates

that the sensor is not very reliable for long-term measurements, as the oxygen concentration is usually calculated from the Stern-Vōlmer plot in these sensors.

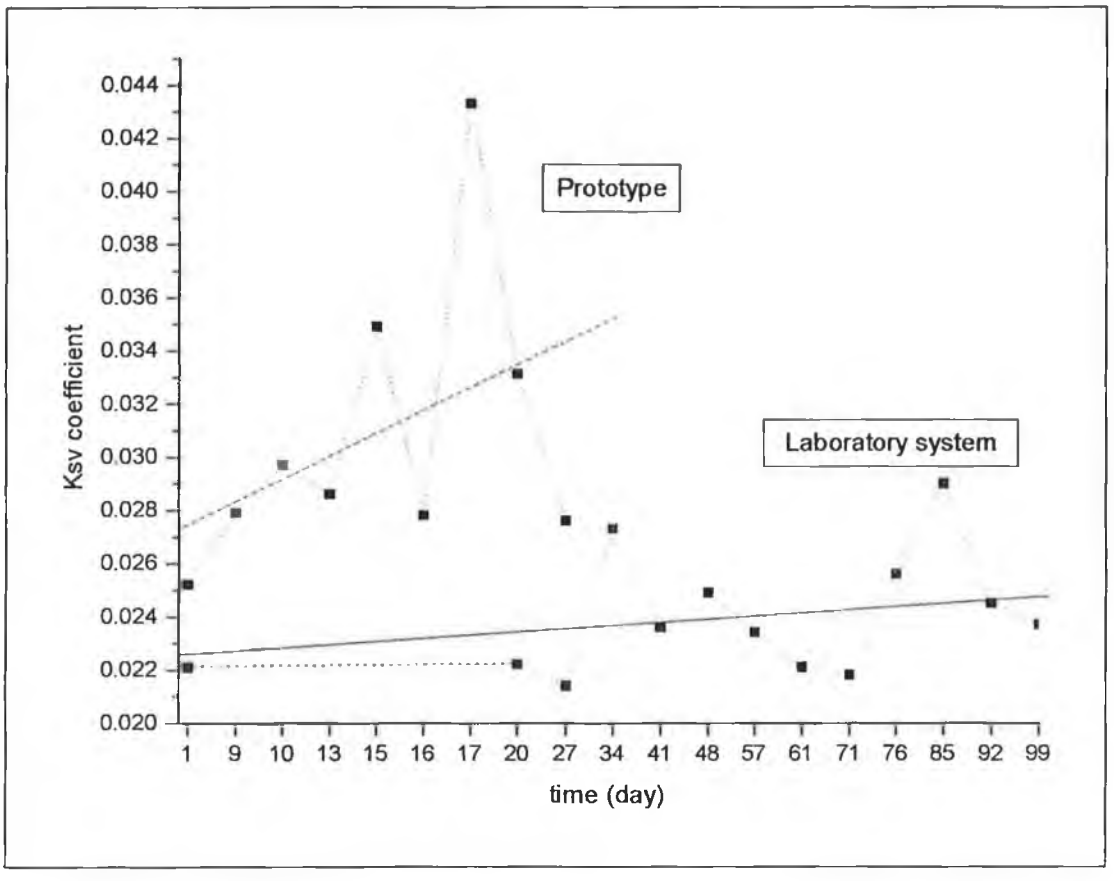

Figure 8.2: Ksv fluctuations over a period of 3 months.

It is clear from Figures 8.1 and 8.2 that, as well as the fluctuation in Q and K_{SV} due to the baseline, there is also a gradual increase in Q and K_{SV} with time. This is thought to be due to a gradual evolution of the film microstructure whereby the pores are opening up due to the fact that the film is stored in water. A more open pore structure would give a higher oxygen diffusion coefficient resulting in higher quenching. This effect is under investigation at present.

8.3 Summary

From the data and discussion presented in Chapters 7 and 8, it is clear that ambient temperature is a major problem in the development of this oxygen sensor. While it was expected that the sensor response would have to be corrected for the temperature dependence of the dye fluorescence and the diffusion coefficient [1], it was not anticipated that the LED temperature dependence would have such a large effect on the baseline stability. Also the influence of sensor design and configuration on temperature effects was not predicted.

It is clear from the work presented here that the laboratory system, consisting of a relatively large sample compartment with LED and photodiode well separated, and these in turn separated from the control electronics, gives reasonably stable and reproducible results. The prototype, on the other hand, being more compact, with the LED and photodiodes enclosed in small metal compartments in close proximity to the control electronics, exhibits baseline drift (mainly due to the LED temperature fluctuations), resulting in an unacceptable lack of reproducibility in quenching response.

The slide mounting configuration in the prototype design also contributed to the lack of reproducibility as it was difficult to insert the slide in exactly the same position each time. This was not a problem in the laboratory system. These insertion problems arose when the design had to allow for the films to be exposed to the environment on the outside of the sensor head.

The problem identified in this phase of the sensor development could be addressed by:

(i) redesigning the sensor head to ensure that the film mounting is reproducible or by designing a disposable screw-on cap with the film permanently secured to it (Cf. Chapter 9).

(ii) finding an alternative LED model with better temperature characteristics. This is not trivial as very few of the major manufacturers have done detailed temperature characterisations and in some cases it is difficult to acquire that information. It would have to be a "trial and error" search. One improved model of LED has already been identified (Cf. Section 7.7).

The major conclusion to come out of this work is that intensity-based oxygen sensing has so many problems associated with it, that the task of producing a commercial oxygen sensor which would produce long-term stable oxygen data would appear to be very difficult. Nevertheless, with improvements discussed above, it may be possible to use this type of sensor in some application where measurement resolution is not an issue.

The concluding chapter (Cf. Chapter 9) discusses an alternative sensor, using the same film type, but monitoring fluorescence decay time instead of fluorescence intensity.

Reference:

[1] A. Mills, Q. Chang, **"Modelled diffusion-controlled response and recovery behaviour of a naked optical film sensor with a hyperbolic-type response to analyte concentration"**, Analyst, 1992, Vol. 117, pp.1461.

Chapter 9: Concluded remarks and future work

9.1 Achievements of objectives

During the course of this project, it became clear that all the objectives stated in Section 2.6 were not going to be achievable within a two-year masters programme. The first two objectives were achieved as the sensor was designed, built and tested under laboratory conditions. Because of the difficulties encountered in the project, an extension to the project has been granted by the funding body.

Unfortunately my contribution to the work has now come to an end but it is satisfying to know that the sensor, after some improvements, will be tested in a pressure vessel in the near future and field tests may follow after that.

9.2 Future work

As stated in the previous section, the sensor will proceed to testing, outside the laboratory environment and hopefully to field testing in the marine environment.

The problems encountered in the development of this marine sensor contributed to a better understanding of issues and limitations associated with intensity-based oxygen sensing. As discussed in Chapter 7 and Chapter 8, improved slide mounting and a more temperature-insensitive LED would vastly improve the performance of the intensity sensor. Another improvement, which is currently under investigation at the moment, is to include an internal reference in the sensor. The aim is to add another component which has the same absorption maximum wavelength as the ruthenium complex, but which is fluorescing at a distinctive wavelength from the ruthenium complex and which is not oxygen sensitive. In this way no calibration is necessary, and any temperature fluctuation is not interfering.

An alternative approach to optical oxygen sensing is to monitor the fluorescence lifetime (Cf. Equation 3.11) instead of intensity (Cf. Equation 3.10). The fluorescence lifetime is an intrinsic property that is independent of fluctuation in light source

intensity, and detection sensitivity. The approach used in another oxygen sensor programme in this laboratory is to monitor the phase shift between the sine-wave modulated fluorescence signal and the reference modulated excitation signal. This phase shift is related to the lifetime and hence can be related to the oxygen concentration. The technique is called phase fluorometry and appears to overcome many of the problems encountered in intensity-sensing. The film is permanently mounted in a screw-on cap which ensures reproducibility of film position. Apart from improved film mounting the phase approach appears to overcome the film insertion problem. This phase sensor is currently being tested.

9.3 Publications arising from the project

C. Malins, S. Fanni, H. G. Glever, J. G. Vos and B. D. MacCraith, **"The preparation of a sol-gel glass oxygen sensor incorporating a covalently bound fluorescent dye"**, Anal. Commun., 1999, 36, pp 3-4.

C. Malins, H. G. Glever, T. E. Keyes, J. G. Vos, W. J. Dressick and B. D. MacCraith, **"Sol-gel immobilised ruthenium(II) polypyridyl complexes as chemical transducers for optical pH sensing"**, Sensors and Actuators B, in press.

APPENDIX

Table A: Measurements taken with the prototype (slide stored in water).

Date	01/07	02/09	10/09	11/09	14/09	16/09	17/09	18/09	21/09	28/09
Ifluo* 100% N2 Ifluo*- Ib before	6.85 6.36	4.25 3.57	3.62 3.11	3.52 3.00	4.26 3.12	3.71 3.32	3.51 2.93	3.56 3.24	3.60 3.14	3.74 2.94
Ifluo* 100% O2 Ifluo*- Ib after	2.47	1.57 0.97	1.23 0.84	1.16 0.80	1.72 0.85	1.19 0.86	1.13 0.84	1.05 0.83	1.30 0.74	1.47 0.81
Ib before Ib after ΔIb in % of Ib average	0.49	0.68 0.60 0.08 **12.5%**	0.51 0.39 0.12 **26.7%**	0.52 0.36 0.16 **36.4%**	1.14 0.87 0.27 **26.9%**	0.39 0.33 0.06 **16.7%**	0.58 0.29 0.29 **66.7%**	0.32 0.22 0.10 **37%**	0.46 0.56 0.10 **19.6%**	0.80 0.66 0.14 **19.2%**
Io before Io after	6.14	 3.35	3.26 3.21	3.28 3.18	3.6 3.31	3.33 3.35	3.47 3.17	3.34 3.47	3.17 3.19	2.85 2.93
K_{sv} before 10^{-4} K_{sv} after 10^{-4} **Δ K_{sv} 10^{-4}** **in % of K_{sv} average**	0.0217	 252	343 279 64 **20.6%**	400 297 103 **29.6%**	492 286 206 **32.4%**	315 349 34 **10.2%**	508 278 230 **58.5%**	350 433 83 **21.2%**	283 331 48 **15.6%**	336 276 60 **19.6%**
Quenching before Quenching after Δ Q in % of Q avearge	68.87	75.49 73.42 2.07 **2.8%**	76.85 73.99 2.86 **3.8%**	78.66 74.68 3.98 **5.2%**	81.41 74.92 6.49 **8.3%**	75.90 74.56 1.34 **1.8%**	81.22 73.91 7.31 **9.4%**	77.47 75.15 2.32 **3.0%**	73.25 75.55 2.3 **3.1%**	77.21 73.70 3.51 **4.6%**

Table B: Measurements taken with the laboratory system (slide stored in water).

Date	04/09/98	21/09	30/09	05/10	12/10	19/10	28/10	01/11	11/11	16/11	23/11	30/11	7/12	23/06/99
Ifluo* 100% N_2	5.18	4.77	5.43	5.24	4.50	7.09	8.01	8.22	7.10	Diff gain	5.36		7.02	4.55
Ifluo*- Ib before	4.50	4.33	4.88	4.74	4.07	6.59	7.45	7.46		2.53	4.93		6.50	4.13
										1.91				
Ifluo* 100% O2	2.05	1.68	2.02	1.83	1.61	2.33	2.74	2.81	2.48	1.14	1.83		2.59	1.57
Ifluo*- Ib after	1.36	1.30	1.50	1.37	1.18	1.83	2.22	2.31	1.92	0.55	1.36		1.79	1.16
Ib before	0.68	0.44	0.55	0.50	0.48	0.50	0.56	0.76		0.62	0.43	0.39	0.52	0.42
Ib after	0.69	0.38	0.52	0.46	0.43	0.50	0.52	0.50	0.56	0.59	0.47	0.38	0.80	0.41
Δ Ib	0.01	0.06	0.03	0.04	0.05	0.00	0.04	0.26		0.03	0.04	0.01	0.28	0.01
in % of Ib average	**1.5%**	**14.6%**	**5.6%**	**8.3%**	**11%**	**0%**	**7.4%**	**41.3%**		**5%**	**9%**	**2.6%**	**42.4%**	
Io before	4.27	4.14	4.66	4.47	3.73	6.35	7.11	7.27			5.34	5.12	6.08	
Io after	4.27	4.16	4.65	4.46	3.94	6.35	7.10	7.35	6.58	1.94	5.34	5.12	6.96	
Ksv before 10^{-4}	219	235	209	240	217	249	229	255			279	247	200	
Ksv after 10^{-4}	221	222	214	273	236	249	234	221	218	256	290	245	237	
Δ Ksv 10-4	2	13	5	33	19	0	5	34			11	2	37	
in % of K_{sv} average	1%	6%	2%	12%	8%	0%	2%	15%			4%	0.8%	17%	
Quenching b	69.55	71.36	69.87	71.94	71.89	72.23	70.74	72.52		72.17	71.60	72.07	68.15	
Quenching a	**69.71**	**70.38**	**69.30**	**71.04**	**71.01**	**72.23**	**71.12**	**70.08**	**70.64**	**71.65**	**72.19**	**71.94**	**71.22**	
Δ Q	0.16	0.98	0.57	0.90	0.88	0	0.38	2.44		0.52	0.59	0.13	3.07	
	0.2%	**1.4%**	**0.8%**	**1.3%**	**1.2%**	**0%**	**0.5%**	**3.4%**		**0.7%**	**0.8%**	**0.2%**	**4.4%**	